VIET NAM NATIONAL UNIVERSITY HO CHI MINH CITY
HO CHI MINH CITY UNIVERSITY OF TECHNOLOGY
FACULTY OF TRANSPORTATION ENGINEERING
DEPARTMENT OF AERONAUTICAL ENEERING

——o0o——

GRADUATION THESIS

A NUMERICAL TOOL USED FOR KINETIC STUDY OF TRANSFORMATION OF METHANE AND CARBON-DIOXIDE BY NON-THERMAL PLASMA

Student: TRUONG The Khai
Stu. ID: 1511544
Supervisor: Assoc.Prof. Vincent ROBIN
Assoc.Prof. NGO Khanh Hieu

Hochiminh city, July 2020

Commitment

I commit that:

- This is the graduation thesis which I have conducted.
- The figures and results stated in the thesis are honest and have not been published in any other works.
- The excerpts and result data used for comparison in this thesis are cited and have the highest accuracy in the scope of my knowledge.

Acknowledgements

First of all, I would express my special thanks of gratitude to my enthusiastic supervisor, *Assoc. Prof. Vincent ROBIN*, who gave me a golden opportunity to take an internship at P' Institute, France. Despite I couldn't come France due to Covid-19 pandemic, he supported me to work from home and helped me to know so many exciting things in numerical method. Although his schedule was so busy, he still took the times to answer my questions as well as gave me the helpful advice, the valuable instructions to complete this study.

I would also pay my deep sense of gratitude to *Dr. LE Thi Hong Hieu* and *Assoc. Prof. NGO Khanh Hieu*, who promoted me for this internship position at P' Institute. They always make as much as possible the best conditions for me throughout the internship.

Furthermore, I would like to acknowledge all teachers at Aeronautical Engineering Department, Ho Chi Minh city University of Technology. They have taught me a lot of extremely useful knowledge, which have become the fundamentals to conduct this study.

I would also thank to one of my best friends, *Mr. PHAN Minh Hai* - student at Department of Advanced Material Technology, Ho Chi Minh city University of Technology, for his helps about chemistry knowledge. He helped me to understand the chemical concepts which I have not ever encountered before.

Lastly, I would love to express my deepest thanks to my family and all my friends who have been by my side. The completion of this thesis could not have been possible without their encouragement.

Sincerely,

Hochiminh city, July 2020.

TRUONG The Khai

Abstract

The subject of this thesis is to generate a numerical tool in order to simulate a Plasma-assisted Plug Flow Reactor with catalyst bed, which is used to reform the Greenhouse gas causing negative impacts on environment actually. This numerical tool is built by solving the fluid describing equations: total mass conservation, mass of species conservation, energy conservation, electron energy conservation.

This thesis concerns on solving the affect of catalyst to the chemical system, and take that affect into numerical model. Furthermore, this thesis also study the numerical method to solve the Boltzmann equation, in order to get the necessary information of plasma for the numerical model. All tools in this thesis were written by Python language using Cantera and Bolos package, and all results were compared with the published references and the reliable software (DETCHEM, BOLSIG+).

Keywords: Reforming greenhouse gas, Catalyst, Numerical modeling, Plasma Physics, Boltzmann equation.

Contents

Nomenclature

Abbreviation

CSTR	Continuous - Stirred Tank Reactor
DR	Dry Reforming Method
EEDF	Electron Energy Distribution Function
PFR	Plug Flow Reactor
POX	Partial Oxidation Method
SR	Steam Reforming Method

Greek Symbols

$\Delta\xi$	The progress of reaction	mol/s
$\dot{\omega}_k$	Net molar production rate of species k per unit volume	$mol/l \cdot s$
Γ_n	Density of sites of phase n	$mol/m2$
$\nu^{'}$, $\nu^{"}$	Stoichiometric coefficient of reactants and productions	
$\sigma_k(n)$	Number of sites that each species k occupies over surface-phase n	
ε	Electron energy	eV
ε_{cat}	Porosity of catalyst bed	

Other Symbols

$[M_k]$	Molar concentration of species k	mol/s
$\boldsymbol{r}$	Position vector of electron	
$\boldsymbol{v}$	Velocity vector of electron	
$\dot{m}$	Mass flow rate	kg/s
$\dot{s_k}$	Net molar production rate of species k per unit area	mol/s
ρ	Mass density of chemical mixture	kg/m^3
B	Magnetic field	T
$C[f]$	Collision term causing the change of EEDF	
c_p	Heat capacity at constant pressure	$J/kg \cdot K$
E	Electrical field	V/m
E/N	Reduced electrical field	$Td,\ 1Td = 10^{-21} V \cdot m^2$
f	Distribution function	
G_k	the rate of formation of species k	mol/s
h	Specific enthalpy	J/kg
k_B	Boltzmann constant	$1.38064852 \times 10^{-23}\, m^2 \cdot kg/s^2 \cdot K$
K_g, K_s	Number of gas-phase and surface-phase species in a chemical system	
k_j	Rate coefficient of a reaction j	
M_k	Chemical symbol of species k	

N_g, N_s	Number of gas-phase and surface-phase reaction in a chemical system	
R	Gas constant	$8.314\, J/mol \cdot K$
r_j	Rate of a reaction j	$mol/l \cdot s$
T	Absolute temperature of gas mixture	K
t	time	s
T_e	Absolute temperature of electron	K or eV
W_k	Molar weight of species k	kg/mol
Y_k	Mass fraction of species k in chemical mixture	
Z_k	Site fraction of surface-phase species k on a surface	

Superscripts

*	Quantity at inlet

Subscripts

e	Indicate electron
g	Indicate gas
j	Reaction j
k	Species k
s	Indicate surface

List of Figures

List of Tables

Chapter 1

Introduction

This chapter will present the impacts of methane and carbon dioxide to the environment, then, the motivation to conduct this subject. The methodology and objectives of this internship will are also introduced.

1.1 Background

1.1.1 Negative Impacts of CO2 and CH4

During the past decades, the rapid development of industries and mega cities have created many advantageous conditions for human. However, be side that, there are also the issues that need to be solved. One of those, global warming has been getting more and more attentions from public concerns, because it has been making a tremendous impact on the world, e.g. the weather conditions is more severe, the natural disasters occur more often with increasingly dangerous levels... For instance, Hurricane Sandy damaged to Jamaica, Cuba, Haiti, the Dominican Republic, The Bahamas, and the U.S. Mid-Atlantic and Northeastern states in late October 2012 [1]. With more than 600,000 housing units were destroyed in New Jersey and New York. The government of New York City estimates that $19 billion in damage and National Geographic

Climate experts predict that extreme weather events like Sandy will become more common as the planet warms [2].

According to the Intergovernmental Panel on Climate Change (IPCC), the increasing emission of greenhouse gases from the factories, the vehicles, as well as the quotidian activities, is the main cause of increasing the severity of global warming [3]. According to the statistics of United States Environmental Protection Agency (EPA) show that the two main greenhouse gases emitted by human activities are CO_2 and CH_4 accounted for 81% and 10%, respectively [4], see Fig.1.1. To reduce the global warming, it requires the solutions focusing on reducing the CO_2 and CH_4 in atmosphere.

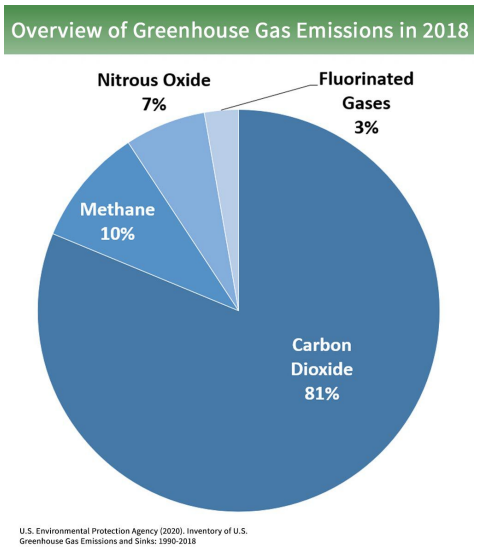

Figure 1.1: Percent of all greenhouse gas emissions from human activities. Source: U. S. Government, Greenhouse Gas Emissions, 2018.

1.1.2 Some Current Solutions

In order to limit their emission, we have to try reducing the source of emission by using as much as possible the renewable energy source to replace the fossil energy source e.g. solar, wind or hydroelectricity. However, according to the report of Eurostat, the consumption of fossil energy source still is a large percent in total [5], see Fig.1.2. So, this solution is not really effective in this time, we need more and more the advanced

science and technology revolutions.

Other solution is more preferable way, that is to treat directly CO_2 and CH_4 existing in nature by transforming into another high valuable chemicals. Indeed, by using the chemical conversions, we can produce the valuable compounds used commonly in industry from carbon dioxide such as urea (Eq.1.1), methanol (Eq.1.2), and formaldehyde (Eq.1.3), etc.

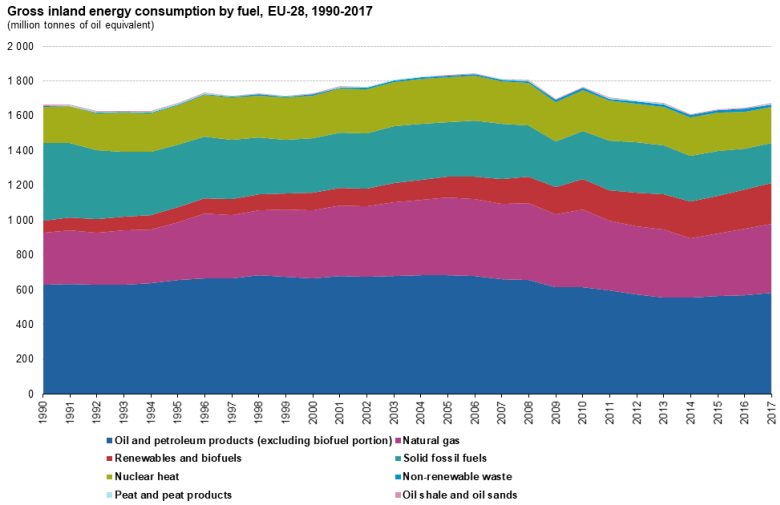

Figure 1.2: Gross inland energy consumption by fuel, EU-28, 1990-2017(million tonnes of oil equivalent) Source: Eurostat, Energy statistic - an overview, 2020.

In recent years, the conversion of light hydrocarbon into synthesis gas or syngas (a gas with H and CO as the main components of fuel) is new trend in 21st century [6], which is a substantial intermediate product in the chemical industry e.g. the synthesis of ethanol and higher alcohols, di-methyl ether and oxo-alcohols, etc. [7] as well as play a improtant role in reducing the negative affects of global warming.

In content of this report, we will focus on the conversion of methane and carbon dioxide into syngas, see *section 1.1.3*.

$$2\,NH_3 + CO_2 \longleftrightarrow \underset{\text{AmmoniumCarbamate}}{NH_2COONH_4} \longleftrightarrow \underset{\text{Urea}}{CO(NH_2)_2} + H_2O \tag{1.1}$$

$$CO_2 + 3\,H_2 \longrightarrow \underset{\text{Methanol}}{CH_3OH} + H_2O \tag{1.2}$$

$$\underset{\text{Methanol}}{2\,CH_3OH} + O_2 \longrightarrow \underset{\text{Formaldehyde}}{2\,CH_2O} + 2\,H_2O \tag{1.3}$$

1.1.3 About the Reforming Methods

The conversion to syngas is called reforming, several technologies have been developed for the reforming of methane. The classic technologies offer syngas with high hydrogen content (Steam Methane Reforming - SMR) or with reduced operating investment (Partial Oxidation - POX) and newer technologies, which are able to consume CO_2 (Dry Methane Reforming - DMR) [7].

Steam Methane Reforming In the 1930s, steam reforming methane is the most important industrial method to manufacture the syngas. The advantage of this method is to the relatively high concentration of hydrogen [8]. However, its disadvantage is not only to require a huge energy supply because this is a high endothermic reaction, but also to be affected by the catalyst deactivation due to carbon formation over catalyst surface [6].

$$CH_4 + H_2O \longleftrightarrow 3\,H_2 + CO\,, \quad \Delta H^0_{298} = 205.9\,\text{kJ/mol}.$$

Dry Reforming Method Despite dry reforming methane produce the production H_2/CO with lower ratio, but this ratio is more suited for the next synthesis process such as oxo synthesis of aldehydes, synthesis of methanol, and acetic acid [9]. Furthermore, this method contribute to convert CO_2, that is why it has gained more attention. Similarly with steam reforming methane, the challenges in dry reforming methane are to need the large energy supply causing high temperature, and the deactivation of

catalyst.

$$CH_4 + CO_2 \longleftrightarrow 2\,H_2 + 2\,CO\,, \quad \Delta H^0_{298} = 247.3\,\text{kJ/mol}.$$

Partial Oxidation A syngas ratios typically of 2 is obtained by using the partial oxidation method, which is most suitable for most downstream processes, such as the direct methanol synthesis. Without catalyst, this process is operated at $1150 - 1500°C$ and $25 - 80bar$, with catalyst the operating condition reducing under $1000°C$ [10]. This method is being developed to reduce the operating condition.

$$CH_4 + \frac{1}{2}O_2 \longleftrightarrow 2\,H_2 + CO\,, \quad \Delta H^0_{298} = -36.0\,\text{kJ/mol}.$$

In order to solve the energy problem, in recent research, plasma was used to reduce the operating temperature, also make sure supply enough energy for reactions, *see chapter 5*. However, there are still many challenges, that was why it requires a kinetics study on these methods to maximise conversion efficiency, to avoid the negative consequences of chemical processes, and to minimise the impact of CO_2 and CH_4 on global warming and climate change.

1.2 Methodology

The long-term objective of this study topic is to develop a complete transformation mechanism of methane and carbon dioxide, therefore, a series of practical experiments would be required, consequently, it spends more cost. To avoid that, a numerical simulation tool is needed to minimise the number of experiments conducted. It is really convenient to determine the optimum operating temperature, to identify the type of catalyst for high performance, to predict the disadvantages of the current practical methods, etc..

Today, with the rapid development of computers, it is possible for us to build a numerical tool to meet those requirements. This numerical simulation tool is the first

step and the basis to achieve the final goal of topic. This tool is built by solving step-by-step the sub-objectives following below:

1. Build a modeling tool, used to simulate a Plug Flow Reactor - PFR, see *section 2.2* and *chapter 4*
2. Develop PFR model (from step 1) to be able to take into account the reactions over catalyst surface, see *section 2.3* and *chapter 4*. This model will simulate three reforming methods presented in *section 1.1.3*.
3. Develop PFR model (from step 2) to be able to take into account the affects of plasma.
   (a) Build a solver to solve Boltzmann Equation describing the characteristics of plasma, see *chapter 5*
   (b) Build a modeling strategy to couple plasma into PFR model, *this is not included in this report*.

The numerical package which we will use for creating this tool is *Cantera* in *Python* environment. This is a powerful toolkit that is used commonly in the Combustion and Chemistry Numerical Research.

1.3 Objective of Internship

In the period of a 4-months internship, I focused on solving the sub-objective number 1 and 2 in *section 1.2*, because the sub-objective number 3 is more complex. It requires more time as well as a more depth study in plasma and numerical modeling method to propose a suitable modeling strategy, therefore, this is beyond the aim of an internship. However, this report will also indicate some main points about plasma, governing equations, etc., that solves the sub-objective 3(a).

Chapter 2

Overview of Chemical Reactor

In this chapter, a summary of chemistry is presented, which consists of the kinetic theory of chemical homogeneous and heterogeneous reactions, the molar conservation to analyse a chemical reactor. The common chemical reactors are also introduced.

2.1 Overview of Chemistry

2.1.1 Chemical Reaction

A chemical reaction is a process transforming from one or more original species (known as reactants) to one or more other species (known as products). It is typically represented by a chemical equilibrium equation (Eq. 2.1) or in another form (Eq. 2.2). The chemical equilibrium equation gives us the proportional qualitative relationships between the species of reaction [11, 12].

$$\nu_A\,A + \nu_B\,B \longleftrightarrow \nu_C\,C + \nu_D\,D \tag{2.1}$$

Where A, B are reactants; C, D are products; ν is stoichiometric coefficient.

$$\begin{aligned} \sum_{k=1}^{N} \nu_k^{'} M_k &\longleftrightarrow \sum_{k=1}^{N} \nu_k^{"} M_k \\ 0 &= \sum_{k=1}^{N} \nu_k M_k \end{aligned} \tag{2.2}$$

Where N is number of species presenting in reaction; M_k is the chemical symbol of species i; $\nu_k^{'}$ and $\nu_k^{"}$ is Stoichiometric coefficient referring to the reactants and productions, respectively; and $\nu_k = \nu_k^{"} - \nu_k^{'}$.

An example from *Cerfacs: Combustion Course* [13], we have a simple reaction below:

$$H_2 + \frac{1}{2}O_2 \longrightarrow H_2O$$

Or we can write in other form:

$$0 = -H_2 - \frac{1}{2}O_2 + H_2O$$

Stoichiometric coefficients of H_2 combustive reaction is shown in Table 2.1.

Table 2.1: Stoichiometric coefficients of H_2 combustive reaction

	H_2	O_2	H_2O
$\nu_k^{'}$	1	1/2	0
$\nu_k^{"}$	0	0	1
ν_k	-1	-1/2	1

2.1.2 Progress of Reaction or Degree of Advancement of Reaction

The progress of reaction, $\Delta\xi$, is ratio of the molar change of species to its stoichiometric coefficient (mol) [11].

$$\Delta\xi = \frac{\Delta n_k}{\nu_k} \tag{2.3}$$

where n_k is mole number of species M_k.

An example from the book *Chimie 1re annee* [11], we have a reaction below:

$$\mathrm{N_2} + 3\,\mathrm{H_2} \longrightarrow 2\,\mathrm{NH_3}$$
$$0 = -\mathrm{N_2} - 3\,\mathrm{H_2} + 2\,\mathrm{NH_3}$$

Table 2.2: Composition of the mixture

Species	$\mathrm{N_2}$	$\mathrm{H_2}$	$\mathrm{NH_3}$
Mole at time t	n_1	n_2	n_3
Mole at time $t + \Delta t$	$n_1 + \Delta n_1$	$n_2 + \Delta n_2$	$n_3 + \Delta n_3$

We have the mole number of species at time t and $t + \Delta t$ in Table 2.2. So, the progress of this reaction that is:

$$\Delta\xi = \frac{\Delta n_1}{-1} = \frac{\Delta n_2}{-3} = \frac{\Delta n_2}{2}$$

2.1.3 Rate of Homogeneous Reaction

We consider a homogeneous phase assumed that is a gas-phase in volume V, having N_g elementary reactions, and K_g species reacting below:

$$\begin{aligned} \sum_{k=1}^{K_g} \nu_{kj}^{'} M_k &\longrightarrow \sum_{k=1}^{K_g} \nu_{kj}^{''} M_k \qquad \text{for} \quad j = 1, .., N_g \\ 0 &= \sum_{k=1}^{K_g} \nu_{kj} M_k \qquad\quad \text{for} \quad j = 1, .., N_g \end{aligned} \tag{2.4}$$

The rate of a homogeneous reaction j, r_j, is the rate of change of the progress of reaction j, $d\xi_j$, per unit time per unit volume through the breaking and subsequent reforming of chemical bonds during the course of the reaction, e.g., in $(mol/dm^3 \cdot s)$.

$$r_j = \frac{1}{V}\frac{d\xi_j}{dt} = \frac{\dot{\xi}_j}{V} \tag{2.5}$$

Rate of a reaction depends on many factors e.g. temperature, molar concentration of species, etc. In general, it can be written as the product of a reaction rate constant, $k(T)$, and a function of the concentrations (activities) of the various species involved in the reaction [14]. To a primary order and reversible reaction (Eq. 2.2), the net reaction rate in form of equation below: (Eq. 2.6).

$$r_j = k_j(T) \cdot \prod_{k=1}^{K_g} [M_k]^{\nu'_{kj}} \tag{2.6}$$

Where, k_j is reaction rate constant of reaction j; $[M_k]$ is molar concentration of species $M_k(mol/dm^3)$.

$$[M_k] = Y_k \rho / W_k \tag{2.7}$$

Where $Y_k = m_k/m$ is the mass fractions with m_k is mass of species M_k present in a given volume V and m is total mass of gas in this volume; ρ is the gas-phase mass density; and the W_k is the molecular weights.

Consequently, *the net volumetric molar production rate* of species M_k, e.g., in $(mol/dm^3 \cdot s)$, equals product of net reaction rate and its stoichiometric coefficient in chemical equilibrium equation.

$$\dot{\omega}_k = \sum_{j=1}^{N_g} \nu_{kj} \cdot r_j = \sum_{j=1}^{N_g} \left(\nu_{kj} k_j(T) \cdot \prod_{l=1}^{K_g} [M_l]^{\nu'_{lj}} \right) \tag{2.8}$$

2.1.4 Reaction Rate Coefficient

The reaction rate constant $k_j(T)$ is is nearly independent of the concentrations of the species involved in the reaction. It is almost always strongly dependent on temperature [14]. Chemist Svante Arrhenius first suggested that the temperature dependence of the specific reaction rate, k(T), could be correlated by the *Arrhenius equation* (Eq. 2.9), has been verified empirically.

$$k_j(T) = AT^B e^{-E_a/RT} \tag{2.9}$$

Where, A is pre-exponential factor or frequency factor;B is the temperature exponent; E_a is activation energy, J/mol or cal/mol; R is gas constant = 8.314 J/mol K = 1.987 cal/mol K; T = absolute temperature, K. All these parameters are called as *Arrhenius parameters*, depending on each specific reaction.

2.2 Chemical reactor

Reactor is a device for containing and controlling a chemical reaction. Depending the conducted method (continue, discontinue, semi-continue) and the states of reactants, products (solid, liquid, gas) we have some types of reactor.

- Discontinue-Flow Reactor: Batch.
- Continue-Flow Reactor: Continuous-Stirred Tank Reactor (CSTR), Plug Flow Reactor (PFR).

We will use the continue flow reactor for our study subject. However, in order to study a reactor, first of all, we need to have a governing equation.

2.2.1 Molar Conservation of Species

In a reactor, we concern on the change of mole number of each species. Similar with evaluation the fluid dynamics, we also use the general conservation law (Eq. 2.10) for a control volume, V, to perform a mole balance on species M_k in a reactor, as shown in Figure 2.1.

$$\frac{\partial}{\partial t}\int_V u dV + \int_S \mathbf{f}\cdot\mathbf{n}\, dS = \int_V q dV \tag{2.10}$$

Mole balance on species M_k at any instant in time, t, yields the following equation:

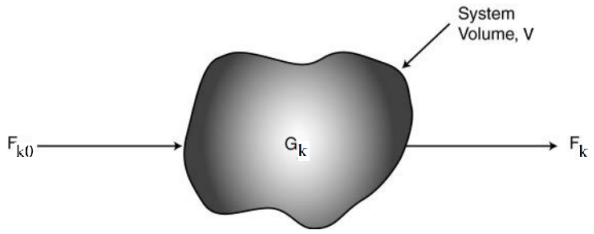

Figure 2.1: Mole balance on species M_k in a system volume, V. Source: H.S.Fogler, *Elements of Chemical Reaction Engineering*, Pearson Education, Inc, 2016.

$$\begin{bmatrix}\text{Rate of flow}\\ \text{of } M_k \text{ into}\\ \text{the system}\\ \text{(moles/time)}\end{bmatrix} - \begin{bmatrix}\text{Rate of flow}\\ \text{of } M_k \text{ out}\\ \text{the system}\\ \text{(moles/time)}\end{bmatrix} + \begin{bmatrix}\text{Rate of generation}\\ \text{of } M_k \text{ by chemical}\\ \text{reaction within}\\ \text{the system}\\ \text{(moles/time)}\end{bmatrix} = \begin{bmatrix}\text{Rate of}\\ \text{accumulation}\\ \text{of } M_k \text{ within}\\ \text{the system}\\ \text{(moles/time)}\end{bmatrix}$$

$$\begin{array}{ccccccc} \textbf{In} & - & \textbf{Out} & + & \textbf{Generation} & = & \textbf{Accumulation} \\ F_{k0} & - & F_k & + & G_k & = & \frac{dn_k}{dt} \end{array} \tag{2.11}$$

The rate of generation of species M_k, G_k equal integral of the rate of formation of species M_k, r_{M_k}, see equation (2.8).

$$G_k = \int_V \omega_k dV \tag{2.12}$$

We replace G_k (Eq. 2.12) into the equation (2.11), we have the equation of mole balance for species M_k, (Eq. 2.13). From this equation, we could calculate and evaluate various types of industrial reactor.

$$F_{k0} - F_k + \int_V \omega_k dV = \frac{dn_k}{dt} \tag{2.13}$$

2.2.2 Continuous-Stirred Tank Reactor (CSTR)

This is a common reactor used in industry, as shown in Figure 2.2 [14], it is normally operated at steady state and is assumed to be perfectly mixed. That is, every variable (temperature, concentration, or reaction rate) independence with time and is the same at every point inside the reactor as well as at the outlet of reactor.

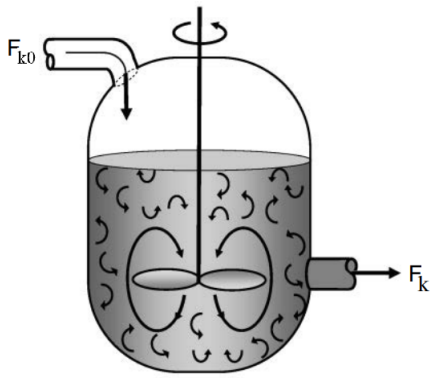

Figure 2.2: Continuous-Stirred Tank Reactor. Source: H.S.Fogler, *Elements of Chemical Reaction Engineering*, Pearson Education, Inc, 2016.

$$\frac{dn_k}{dt} = 0 \tag{2.14}$$

$$\int_V \omega_k dV = V\omega_k \tag{2.15}$$

The general mole balance equation (2.13) is applied to a CSTR operated at steady state (Eq. 2.14), and there are no spatial variations in the rate of reaction (Eq. 2.15), we have equation (2.16):

$$V = \frac{F_{k0} - F_k}{-\omega_k} \tag{2.16}$$

2.2.3 Plug Flow Reactor (PFR)

Plug Flow Reactor consists of a cylindrical pipe, is shown in Figure 2.3 [14], and is normally operated at steady state, as is the CSTR. It are used most often for gas-phase reactions. The reaction occur continuously as they flow down the length of the reactor. We assume that the flow profile in reactor is uniform, therefore, every variables only depend on the axial direction through the reactor (no radial variation).

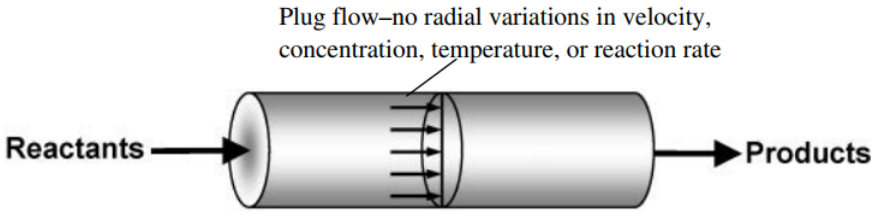

Figure 2.3: Plug Flow Reactor. Source: H.S.Fogler, *Elements of Chemical Reaction Engineering*, Pearson Education, Inc, 2016.

We divide the plug flow reactor into the differential volume, ΔV, so small that there are no spatial variations of variable, see Figure 2.4 [14]. Thus the generation term, ΔG_k, equals

$$\Delta G_k = \int_{\Delta V} \omega_k dV = \omega_k \Delta V$$

So, the general mole balance equation is applied to volume ΔV operated at steady state, that is:

$$F_k\big|_V - F_k\big|_{V+\Delta V} + \omega_k \Delta V = 0$$

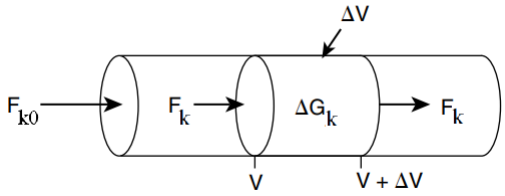

Figure 2.4: Mole balance on species M_k in volume ΔV. Source: H.S.Fogler, *Elements of Chemical Reaction Engineering*, Pearson Education, Inc, 2016.

Rearranging,

$$\frac{F_k\big|_{V+\Delta V} - F_k\big|_V}{\Delta V} = \dot{\omega_k} \tag{2.17}$$

With ΔV closes zero, the left hand side of equation (2.17) will become the differential form.

$$\frac{dF_k}{dV} = \dot{\omega_k} \tag{2.18}$$

2.2.4 Approximating a PFR by a Large Number of CSTRs in Series

From the assumptions of PFR reactor in *section 2.2.3*, approximately, we can consider that a PRF reaction is equivalent with a series of CSTR reactors having the small, equal - volumes, ΔV, see Figure 2.5 [14]. It is proofed mathematically in equation (2.19) from two molar conservation equation of each type of reactor (Eq. 2.16) and (Eq. 2.18)

By integrate equation (2.18), we will determine the mole rate at outlet of PFR reactor. Then use relationship formula of integral and summary, we will proof the approximation between PFR and series of CSTR.

$$[F_k - F_{k0}]_{\text{PFR}} = \int_V \dot{\omega_k} dV = \sum_{j=1}^{N} \dot{\omega_k}^j \Delta V = \sum_{j=1}^{N} [F_k - F_{k0}]^j_{\text{CSTR}} \tag{2.19}$$

Where N is number of equivalent CSTR reactors; j indicates jth reactor in series.

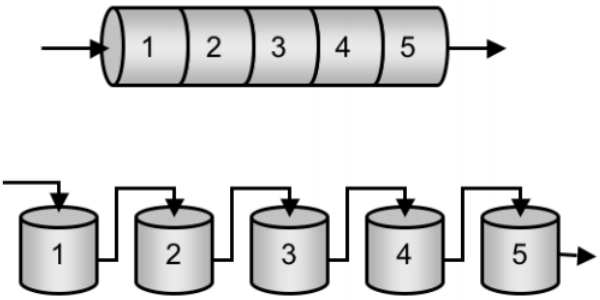

Figure 2.5: Modeling a PFR with CSTRs in series. Source: H.S.Fogler, *Elements of Chemical Reaction Engineering*, Pearson Education, Inc, 2016.

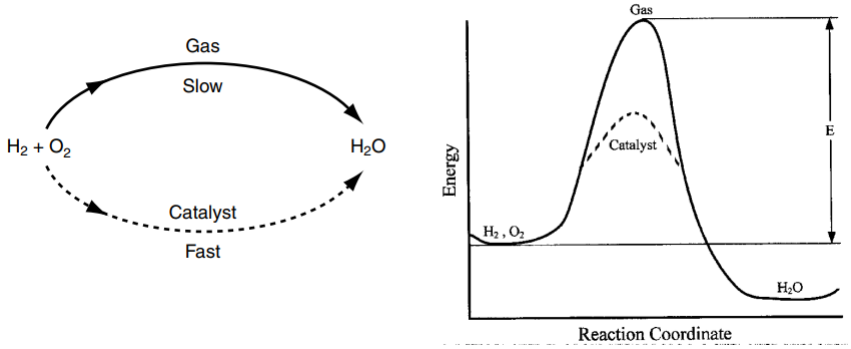

Figure 2.6: Different reaction paths. Source: H.S.Fogler, *Elements of Chemical Reaction Engineering*, Pearson Education, Inc, 2016.

Therefore, we can model a PFR with a large number of CSTRs in series. We will discuss the reason why use this approximation in the following chapter.

2.3 Catalyst

Catalyst is substance added into the reaction, which provides an alternative reaction pathway with a lower activation energy than the non-catalyzed reaction mechanism. Consequently, the catalyst will accelerate the rate of reaction without being changed themselves by the reaction [11]. For example, reaction $H_2 + \frac{1}{2}O_2 \longrightarrow H_2O$ with and without the catalyst, is shown in Figure 2.6 [14].

There are two type of catalyst:

- Homogeneous Catalyst: the phase of catalyst is the same as the phase of reactants. In this case, reaction is accelerated in the whole of volume.
- Heterogeneous Catalyst: the phase of catalyst is different from the phase of reactants. In heterogeneous catalyzed reaction, the reaction is accelerated on the surface of catalyst.

In this study about conversion of syngas or reforming (see *section 1.1.3*), we use the heterogeneous catalyst, Nickel (solid) in particular. With the presence of catalyst, there are some new species in reaction mechanism. Those new species are formed over the catalyst surface by the reactions between gas and solid (heterogeneous reactions), are known as surface-phase species.

For example, we have two gas species H_2, O_2 and one surface species $Ni(s)$. There are heterogeneous reactions, is shown in Table 2.3, where (s) indicates surface. It consists of two type of reaction, one is stick reaction which makes the gas species stick over surface species, another is surface reactions where occurs the reaction between the surface species.

Table 2.3: Heterogeneous reactions of H_2 and O_2 over Ni

Reaction	**Type**
$H_2 + 2\,Ni(s) \longrightarrow 2\,H(s)$ $O_2 + 2\,Ni(s) \longrightarrow 2\,O(s)$	Stick Reaction
$2\,H(s) + 2\,Ni(s) \longrightarrow H_2$ $2\,O(s) + 2\,Ni(s) \longrightarrow O_2$ $H(s) + O(s) \longrightarrow OH(s) + Ni(s)$ $OH(s) \longrightarrow H(s) + O(s) + Ni(s)$	Surface Reaction

2.3.1 Heterogeneous Reaction

We consider N_s heterogeneous reactions consists K_g species in a gas-phase, n_s phase of surface and $K_s(n)$ species on surface-phase n (Eq. 2.20).

$$\begin{aligned} \sum_{k=1}^{K_g+K_s} \nu_{kj}^{'} M_k \longrightarrow \quad & \sum_{k=1}^{K_g+K_s} \nu_{kj}^{''} M_k \quad \text{for} \quad j = 1, .., N_s \\ 0 = \quad & \sum_{k=1}^{K_g+K_s} \nu_{kj} M_k \quad \text{for} \quad j = 1, .., N_s \end{aligned} \tag{2.20}$$

In work of *Coltrin et al.* [15], each surface species occupies one or more surface *sites*. A site is considered to be a location or position on the surface at which a species can reside. A site does not necessarily have to be a particular atom or have a composition itself. There can be any number of types of sites on the surface. We consider each surface site type to be a "phase". A given chemical species only resides on one type of site. The population of different species occupying a given type of site is conveniently specified by site fractions, Z_k. By definition the sum of the site fractions of the species on a given type of site is unity. The total number of surface species on site type n is $K_s(n)$, and they are numbered sequentially from the first species $K_s^f(n)$ to the last species $K_s^l(n)$.The total number of surface species in all phases is K_s. Each surface site-type or phase must contain one or more species

The site fractions on each site type (surface phase) are normalized:

$$\sum_{k=K_S^f(n)}^{K_S^l} Z_k(n) = 1 \tag{2.21}$$

The surface molar concentration of a species is then

$$[M_k] = \frac{Z_k(n)\Gamma_n}{\sigma_k(n)} \tag{2.22}$$

where Γ_n, is the density of sites of phase n (in mol/cm^2)and $\sigma_k(n)$ is the number of sites that each species M_k occupies.

Consider the simple system in Figure 2.7, a surface consisting of only four sites and two species. In this example two of the sites are occupied by SiH_4 molecules (with $\sigma_k = 1$)and the other two sites are occupied by a single Si_2H_6 molecule (with $\sigma_k = 2$). In our formalism the site fraction of each molecule is 0.5. That is, half of the sites are occupied by each species. As is seen in equation (2.22) it is necessary to divide the site fraction of each species by σ_k to convert to a concentration.

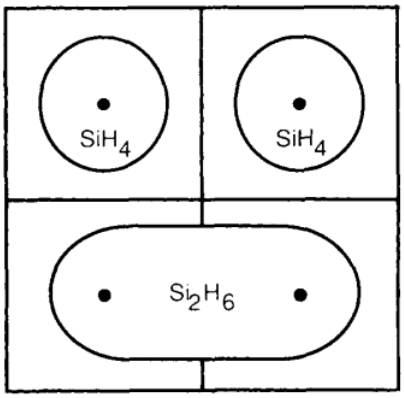

Figure 2.7: Simple example of a system consisting of four sites and two species. Source: M.E.Coltrin et al, from *Chemical Kinetics*, vol. 23, 1991.

2.3.2 Rate of Heterogeneous Reaction

The molar rate of these heterogeneous reactions, depend on the surface of catalyst, A, contacting with gas phase. Therefore, the net molar production rate of species M_k is the change of mole per unit time per unit area due to heterogeneous reaction,e.g., in mol/m^2s. This net molar production rate, $\dot{s_k}$, is calculated in analogy to homogeneous reactions as a product of rate coefficients and concentrations:

$$\dot{s_k} = \sum_{j=1}^{N_s} \nu_{kj} \cdot r_j = \sum_{j=1}^{N_s} \nu_{kj} \left(k_j(T) \cdot \prod_{k=1}^{K_g+K_s} [M_k]^{\nu_k'} \right) \tag{2.23}$$

where r_j is rate of heterogeneous reactions; $[M_k]$ is concentration of species M_k, $[M_k] = Y_k\rho/W_k$ in (mol/dm^3) for gas-phase species, and $[M_k] = Z_k(n)\Gamma_n/\sigma_k(n)$ in (mol/m^2) for surface-phase species; and the heterogeneous rate constant, $k_j(T)$, depends on type of heterogeneous reaction.

Rate Constant of Stick Reaction

Stick reaction is the result of collisions between gas-phase molecules and surfaces which result in the gas- phase molecule sticking to the surface. Thus, the rate constant of stick reaction depends on a sticking coefficient, γ, by the formula:

$$k_j = \frac{\gamma}{\Gamma^m}\sqrt{\frac{RT}{2\pi W_k}} \tag{2.24}$$

Where Γ is the molar site density; m is the sum of all the surface reactant stoichiometric coefficients; W_k is the molecular weight of the gas phase species; and stick coefficient, γ, equals

$$\gamma = aT^b e^{-c/RT} \tag{2.25}$$

where a, b, c are constants specific to the reaction

Rate Constant of Surface Reaction

The rate constant of surface reactions, $k_j(T)$, are represented by an extended Arrhenius-like rate expression, which combines the modified Arrhenius rate expression with further corrections dependent on the fractional surface coverage Z_k of one or more surface species (Eq. 2.26).

$$k_j(T) = AT^b \exp\left(-\frac{E_a}{RT}\right)\prod_k 10^{a_k\theta_k}\theta_k^{m_k}\exp\left(\frac{-E_k Z_k}{RT}\right) \tag{2.26}$$

where A, b and E_a are the Arrhenius parameters presented in equation (2.9); a_k, m_k, E_k and are the coverage dependencies from species.

2.4 Summary

If we have a chemical system, in which consists of one gas-phase having K_g gas species, N_g homogeneous reactions, and n surface phase having totally K_s surface species, N_s heterogeneous reactions, we could determine the generation term G_k of species M_k in the molar balance equation by equation (2.27).

$$G_k = \int_V \omega_k dV + \int_S \dot{s_k} dS \tag{2.27}$$

Where ω_k and $\dot{s_k}$ is summarised in Table 2.4 and Table 2.5.

Type of Reaction	**Net Molar Production Rate**
Homogeneous	$\dot{\omega}_k = \sum_{j=1}^{N_g} \dot{\omega}_{kj} = \sum_{j=1}^{N_g} \left(\nu_{kj} k_j(T) \cdot \prod_{l=1}^{K_g} [M_l]^{\nu'_{lj}} \right)$
Heterogeneous	$\dot{s}_k = \sum_{j=1}^{N_g} \dot{s}_{kj} = \sum_{j=1}^{N_g} \left(\nu_{kj} k_j(T) \cdot \prod_{l=1}^{K_g+K_s} [M_l]^{\nu'_{lj}} \right)$

Table 2.4: Summary of net molar production rate formula

Type of Reaction	**Molar Concentration**	**Rate Constant**
Homogeneous	$[M_l] = Y_l \rho / W_l$	$k_j(T) = A e^{-E_a/RT}$
Heterogeneous	$[M_l] = Y_l \rho / W_l$ (for gas species)	$k_j = \frac{\gamma}{\Gamma^m} \sqrt{\frac{RT}{2\pi W_k}}$ (for stick reactions)
	$[M_k] = \frac{Z_k(n)\Gamma_n}{\sigma_k(n)}$ (for surface species)	$k_j(T) = AT^b \exp\left(-\frac{E_a}{RT}\right) \prod_k 10^{a_k \theta_k} \theta_k^{m_k} \exp\left(\frac{-E_k Z_k}{RT}\right)$ (for surface reactions)

Table 2.5: Summary of Concentration and Rate Constant

Chapter 3

Zero-Dimensional Reactor Model

We will derive the governing equations for simulating a 0D reactor taking the affect of catalyst into account. Cantera toolkit providing interfaces for modeling complex chemical reaction system will be also introduced

3.1 An overview

In practical, the plug flow reactor (PFR) is used for reforming process, having a constant volume, added the catalyst inside. It operates at steady state under a constant pressure. In the axial direction z, the states of the gas is allowed to change. However, all diffusion processes are neglected. The governing equations of Plug-Flow Reactors are [16].

Mass conservation

$$\frac{d(\rho u S)}{dz} = A \sum_k \dot{s}_k W_k \tag{3.1}$$

Where, u is the axial velocity in (m/s), S is cross-sectional area of PFR reactor.

Continuity equation of species

$$\rho u \frac{dY_k}{dz} + Y_k A \sum_k \dot{s}_k W_k = \dot{\omega}_k W_k + A \dot{s}_k W_k \tag{3.2}$$

Energy conservation

$$\rho u S c_p \frac{dT}{dz} = -S \sum_k h_k \dot{\omega}_k W_k - A \sum_k h_k \dot{s}_k W_k - \dot{Q} \tag{3.3}$$

Momentum conservation in the axial direction

$$\rho u S \frac{du}{dz} + u A \sum_k \dot{s}_k W_k = -\frac{d(pS)}{dz} - \tau_w A \tag{3.4}$$

A Plug-Flow Reactor can also be described from a Lagrangian point of view. An unsteady fluid particle is considered which travels along the axial streamline through the PFR. Since there is no information traveling upstream, the state change of the fluid particle can be computed by a forward (upwind) integration in time. Using the continuity equation, the speed of the particle can be derived. By integrating the velocity in time, the temporal information can be translated into the spatial resolution of the PFR [17].

Even though this problem extends geometrically in one direction, *it can be modeled via zero-dimensional reactors*. Due to the neglecting of diffusion, downstream parts of the reactor have no influence on upstream parts. The Plug-Flow Reactor is spatially discretized into a large number of axially distributed volumes. These volumes are modeled to be steady-state CSTRs, see Figure 3.1 [17, 18].

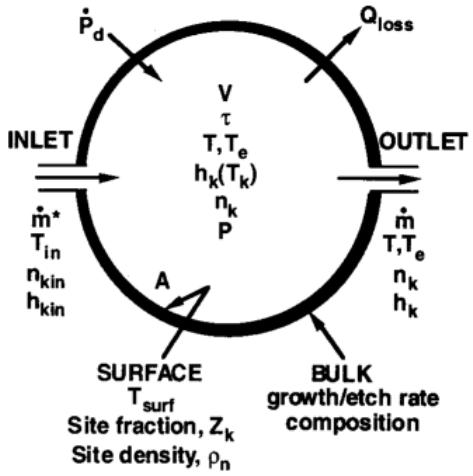

Figure 3.1: Schematic representation of a well stirred reactor. Source: E.Meeks and J.W.Shon, from *Transactions on Plasma Science*, vol. 23, 1995.

Moreover, in the plasma-assisted reactor (final objective of subject), the macroscale fluid modelling is one of the challenges due to the complex phenomenon of plasma. Currently, most of the macroscale models are zero-dimensional (0D), and the species densities are calculated by using balance equation based on the production/loss processes as a function of time [19].

The 0D models are time-efficient and capable of explaining the plasma chemistry, this computational model can handle a large of species, the detailed chemical reaction mechanisms or complex reactor networks [19]. The contents and its properties of 0D reactor are assumed to be nearly spatially uniform due to high diffusion rates or forced turbulent mixing. This is a very good assumption for the low-pressure, highly diffuse operating conditions of most plasma-etch reactors [20].

3.2 Governing Equations of 0D reactor

The following equations represent the transient conservation equations for the well stirred reactor, having volume V and surface area of catalyst A. In this reactor, there are K_g gas-phase species, K_s surface-phase species reacting, and N reactions in total

(N_g homogeneous reactions and N_s heterogeneous reactions).

$$\begin{aligned} &\sum_{k=1}^{K_g+K_s} \nu'_{kj} \quad M_k \longleftrightarrow \sum_{k=1}^{K_g+K_s} \nu''_{kj} M_k \quad \text{for } j = 1, N \\ &\text{Or} \qquad\qquad 0 = \sum_{k=1}^{K_g+K_s} \nu_{kj} M_k \qquad\quad \text{for } j = 1, N \end{aligned} \tag{3.5}$$

We have to solve the variables at out flow consisting of the gas density, ρ; the gas temperature, T; the mass fraction of gas-phase species, Y_k and the site fraction of surface-phase species, Z_k from N homogeneous and heterogeneous reactions. Thus, we have totally $K_g + K_s + 2$ variables, so, we need to build $K_g + K_s + 2$ equations of conservation.

3.2.1 Mass Conservation

Global mass conservation in the reactor volume, where the time-rate of change of mass in the the reactor equals to the difference between the mass flow in and the mass flow out, plus the net mass loss from the surfaces by chemical reaction.

$$\frac{d}{dt}(\rho V) = \dot{m}^* - \dot{m} + \sum_{k=1}^{K_g} \dot{s}_k W_k A \tag{3.6}$$

Where ρ is the mass density; $\dot{m}^*$ is the mass flow rate into reactor, and $\dot{m}$ is the outlet flow rate; $\dot{s}_k = \sum_{j=1}^{N_s} \dot{s}_{kj}$ (Eq. 2.23) is the net molecular production rate of species M_k per unit area due to heterogeneous reactions; W_k is the molecular mass of species M_k.

3.2.2 Gas-phase Species Conservation

The time-rate of change of mass of gas-phase species M_k in the the reactor equals to the difference between its mass flow in and its mass flow out, plus the net mass change of species M_k from the surfaces by heterogeneous reactions (gas-solid reactions) and

homogeneous reactions (gas-gas reactions).

$$\begin{aligned} &\frac{d}{dt}(m_k) = \dot{m}_k^* - \dot{m}_k + \dot{s}_k W_k A + \dot{\omega}_k W_k V \qquad \text{for} \quad k = 1..K_g \\ \Longleftrightarrow\ &\frac{d}{dt}(\rho V Y_k) = \dot{m}^* Y_k^* - \dot{m} Y_k + \dot{s}_k W_k A + \dot{\omega}_k W_k V \qquad \text{for} \quad k = 1..K_g \end{aligned} \tag{3.7}$$

Where $\dot{m}_k^*$ and $\dot{m}_k$ are mass flow rate of species M_k at inlet and outlet, respectively; $\dot{\omega}_k = \sum_{j=1}^{N_g} \dot{\omega}_{kj}$ (Eq. 2.8) is the net volumetric molecular production rate of species M_k due to gas-phase reactions.

Replacing $\dot{m}$ from equation (3.6), and expand the we have

$$\begin{aligned} \rho V \frac{\partial Y_k}{\partial t} + Y_k \frac{\partial (\rho V)}{\partial t} = \dot{m}^* Y_k - \Big(\dot{m}^* - \frac{\partial (\rho V)}{\partial t} + \sum_{j=1}^{K_g} \dot{s}_j W_j A \Big) Y_k \\ + \dot{s}_k W_k A + \dot{\omega}_k W_k V \quad \text{for} \quad k = 1..K_g \end{aligned} \tag{3.8}$$

Rearranging, we have the gas species conservation equation (3.9)

$$\rho V \frac{\partial Y_k}{\partial t} = \dot{m}^* (Y_k^* - Y_k) - Y_k \Big(\sum_{j=1}^{K_g} \dot{s}_j W_j A \Big) + \dot{s}_k W_k A + \dot{\omega}_k W_k V \quad \text{for} \quad k = 1..K_g \tag{3.9}$$

3.2.3 Surface Species Conservation

We consider the balance equation between the time rate of change of each surface species concentration with the net production rate of that surface species through chemical reactions at the surface.

$$\frac{d}{dt}(A[M_k]W_k) = A W_k \dot{s}_k \quad \text{for} \quad k = 1..K_s \tag{3.10}$$

Replacing the molar concentration of a surface species, $[M_k]$ is defined from equation (2.22), $[M_k] = \Gamma Z_k / \sigma_k$, we have

$$\begin{aligned} & \frac{d}{dt}\left(A\frac{\Gamma Z_k}{\sigma_k}W_k\right) = AW_k\dot{s}_k && \text{for} \quad k = 1..K_s \\ \Longleftrightarrow \quad & \frac{\partial Z_k}{\partial t} = \sigma_k\frac{\dot{s}_k}{\Gamma} - \frac{Z_k}{\Gamma}\frac{\partial \Gamma}{\partial t} && \text{for} \quad k = 1..K_s \end{aligned} \tag{3.11}$$

The rate of change of site density Γ for surface phase, in $mole/cm^2$, is equation (3.12).

$$\frac{\partial \Gamma}{\partial t} = \sum_{k=1}^{K_s} \sigma_k \dot{s}_k \tag{3.12}$$

However, in our study, we assume that the site density is constant, thus this term will be zero. Finally, the surface species conservation equation is,

$$\frac{\partial Z_k}{\partial t} = \sigma_k\frac{\dot{s}_k}{\Gamma} \quad \text{for} \quad k = 1..K_s \tag{3.13}$$

3.2.4 Energy Conservation

Rate of change of enthalpy of system consists of rate of change of enthalpy of gas-phase and rate of change of enthalpy of surface-phase, plus energy exchange to environment.

$$\frac{dH_{sys}}{dt} = \frac{dH_g}{dt} + \frac{dH_s}{dt} - \dot{Q} + \dot{P}_d \tag{3.14}$$

Surface-phase energy

The rate of change of surface-phase enthalpy only equal the energy produced by the heterogeneous reactions.

$$\frac{dH_s}{dt} = A\sum_{k=1}^{K_s} \dot{s}_k W_k h_k \tag{3.15}$$

Where K_s is number of surface-phase species.

Gas-phase energy

The rate of change of enthalpy of gas-phase equal the difference between enthalpy of flow in and enthalpy of flow out, plus the change of enthalpy by chemical reaction.

$$\frac{dH_g}{dt} = \dot{m}^* \sum_{k=1}^{K_g} Y_k^* h_k^* - \dot{m} \sum_{k=1}^{K_g} Y_k h_k + A \sum_{k=1}^{K_g} \dot{s}_k W_k h_k + V \sum_{k=1}^{K_g} \dot{\omega}_k W_k h_k \tag{3.16}$$

Where h_k^* and h_k is specific enthalpy of gas-phase species M_k at inlet and outlet, respectively; K_g is number of gas-phase species.

With some mathematical steps, and use the definition of averaged enthalpy, $\bar{h} = \sum_{k=1}^{K_g} Y_k h_k$, the left hand side (L.H.S) of equation (3.16) become:

$$\frac{dH_g}{dt} = (\rho V)\frac{\partial \bar{h}}{\partial t} + \bar{h}\frac{\partial(\rho V)}{\partial t}$$

$$\Longleftrightarrow \frac{dH_g}{dt} = (\rho V) \sum_{k=1}^{K_g} \left(h_k \frac{\partial Y_k}{\partial t} \right) + (\rho V) \sum_{k=1}^{K_g} \left(Y_k c_{pk} \frac{\partial T_k}{\partial t} \right) + \sum_{k=1}^{K_g} Y_k h_k \frac{\partial(\rho V)}{\partial t}$$

Assume that system is thermal, all gas-phase species, T_k, equal the gas temperature, T. And use definition of averaged heat capacity, $\bar{c}_p = \sum_{k=1}^{K_g} Y_k c_{pk}$, we have the enthalpy equation of gas-phase (Eq. 3.17).

$$\frac{dH_g}{dt} = (\rho V) \sum_{k=1}^{K_g} \left(h_k \frac{\partial Y_k}{\partial t} \right) + \rho V \bar{c}_p \frac{\partial T}{\partial t} + \sum_{k=1}^{K_g} Y_k h_k \frac{\partial(\rho V)}{\partial t} \tag{3.17}$$

Replacing equation (3.15) and equation (3.17) into equation (3.14), and rearranging, we have,

$$\begin{aligned} \rho V \bar{c}_p \frac{\partial T}{\partial t} =& \dot{m}^* \sum_{k=1}^{K_g} Y_k^* h_k^* - (\rho V) \sum_{k=1}^{K_g} \left(h_k \frac{\partial Y_k}{\partial t} \right) - \sum_{k=1}^{K_g} (Y_k h_k) \left(\frac{\partial(\rho V)}{\partial t} + \dot{m} \right) \\ &+ A \sum_{k=1}^{K_g + K_s} \dot{s}_k W_k h_k + V \sum_{k=1}^{K_g} \dot{\omega}_k W_k h_k \end{aligned} \tag{3.18}$$

In the right hand side of equation (3.18), the second term of is expanded from equation (3.9) multiplied by h_k; and the third term is transformed from global mass conservation (Eq. 3.6).

$$
\begin{aligned}
(\rho V)\sum_{k=1}^{K_g} h_k \frac{\partial Y_k}{\partial t} &= \sum_{k=1}^{K_g}\left[\dot{m}^* h_k (Y_k^* - Y_k) - Y_k h_k \left(\sum_{k=1}^{K_g} \dot{s}_k W_k A\right) + \dot{s}_k W_k h_k A + \dot{\omega}_k W_k h_k V\right] \\
&= \sum_{k=1}^{K_g} \dot{m}^* h_k (Y_k^* - Y_k) - \sum_{k=1}^{K_g} (Y_k h_k) \cdot \sum_{k=1}^{K_g} (\dot{s}_k W_k A) \\
&\quad + A\sum_{k=1}^{K_g} \dot{s}_k W_k h_k + V \sum_{k=1}^{K_g} \omega_k W_k h_k
\end{aligned}
$$

$$
\begin{aligned}
\sum_{k=1}^{K_g} (Y_k h_k)\left(\frac{\partial(\rho V)}{\partial t} + \dot{m}\right) &= \sum_{k=1}^{K_g} (Y_k h_k)\left(\dot{m}^* + \sum_{k=1}^{K_g} \dot{s}_k W_k A\right) \\
&= \dot{m}^* \sum_{k=1}^{K_g} Y_k h_k + \sum_{k=1}^{K_g} (Y_k h_k) \cdot \sum_{k=1}^{K_g} (\dot{s}_k W_k A)
\end{aligned}
$$

After replacing and simplifying, we have the energy conservation in a more simple equation (3.19).

$$
\rho V \bar{c}_p \frac{\partial T}{\partial t} = \dot{m}^* \sum_{k=1}^{K_g} Y_k^* (h_k^* - h_k) - V \sum_{k=1}^{K_g} \dot{\omega}_k W_k h_k - A \sum_{k=1}^{K_g+K_s} \dot{s}_k W_k h_k - \dot{Q} + \dot{P}_d \quad (3.19)
$$

3.3 Cantera

Cantera is an open-source simulation toolkit, developed originally by Prof. *Dave Goodwin (1957–2012)* [17]. It provides object-oriented modules and library functions that can be used either from scripting software like Python and MATLAB, or applications written in C++ and Fortran. Cantera is an open-source alternative to commercial codes like CHEMKIN [21] and DETCHEM [22] that provides interfaces for modeling complex chemical reaction systems and their underlying thermodynamics, kinetics and transport.

3.3.1 Structure of Cantera

Cantera offers some common available models that are very helpful for users, e.g., equilibrium state calculation, constant pressure/Volume batch reactor, burner stabilized and propagating premixed flat flame. In order to run a simulation program using Cantera with Python, we need to have the data files, and the simulation scripts, see the flowchart in Figure 3.2.

Data File

The data files in format *.cti* or *.xml* consist of the information about:

- Phases and interfaces information (species involved, thermodynamics model, ...)
- Elements and species data (composition, thermodynamics data, ...)
- Reaction data (chemical expression, rate coefficient, ...)

Simulation Script

The simulation script is written in Python environment, which calls the functionalities object of Cantera as well as permit the users to be able to modify and to develop these objects for each particular simulation requirement.

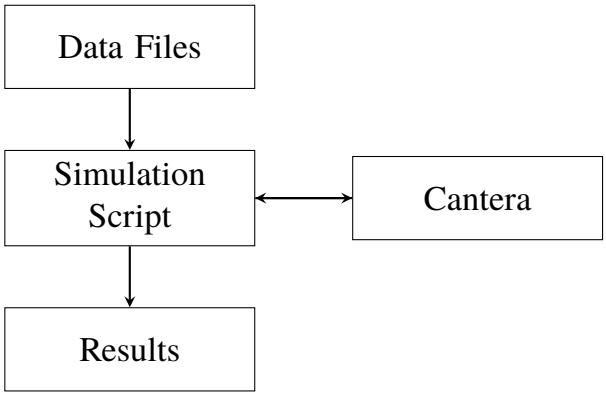

Figure 3.2: Structure of Cantera in Python environment

3.3.2 Numerical Methods

Cantera provides an ODE solver for solving the equations of reacting systems that is SUNDIALS solver [23]. SUNDIALS is a *SUite of Nonlinear and DIfferential/ALgebraic equation Solvers* with the goal of providing robust time integrators and nonlinear solvers that can easily be incorporated into existing simulation codes. It consists of the following six solvers: **CVODE**, solves initial value problems for ordinary differential equation (ODE) systems; **CVODES**, solves ODE systems and includes sensitivity analysis capabilities (forward and adjoint); **ARKODE**, solves initial value ODE problems with additive Runge-Kutta methods, include support for IMEX methods; **IDA**, solves initial value problems for differential-algebraic equation (DAE) systems; **IDAS**, solves DAE systems and includes sensitivity analysis capabilities (forward and adjoint); **KINSOL**, solves nonlinear algebraic systems.

In this work, a simulation of reactor, Catera will use **CVODE** solver from SUNDIALS [17] to solve the initial value problem (Eq. 3.20). CVODE uses time-step scheme is that the Backward Differentiation Formulas (BDFs) having the general implicit formula in equation (3.21) [24, 25], and uses the Newton iteration to solve approximately the implicit nonlinear systems within implicit integrators at each integration step.

$$y' = f(t, y), \quad y(t_0) = y_0 \tag{3.20}$$

$$\sum_{k=0}^{s} a_k y_{n+k} = h\beta f(t_{n+s}, y_{n+s}) \tag{3.21}$$

where h denotes the step size and $t_n = t_0 + nh$. Since f is evaluated for the unknown y_{n+s}, BDF methods are implicit and possibly require the solution of nonlinear equations at each step. The coefficients a_k and β are chosen so that the method achieves order s, which varies between 1 and 5 to ensure the stability of numerical method.

The formulas for order from 1 to 5 are following below [24]:

- BDF order 1: $y_{n+1} - y_n = hf(t_{n+1}, y_{n+1})$ (this is the backward Euler method)

- BDF order 2: $y_{n+2} - \frac{4}{3}y_{n+1} + \frac{1}{3}y_n = \frac{2}{3}hf(t_{n+2}, y_{n+2})$
- BDF order 3: $y_{n+3} - \frac{18}{11}y_{n+2} + \frac{9}{11}y_{n+1} - \frac{2}{11}y_n = \frac{6}{11}hf(t_{n+3}, y_{n+3})$
- BDF order 4: $y_{n+4} - \frac{48}{25}y_{n+3} + \frac{36}{25}y_{n+2} - \frac{16}{25}y_{n+1} + \frac{3}{25}y_n = \frac{12}{25}hf(t_{n+4}, y_{n+4})$
- BDF order 5:

  $y_{n+5} - \frac{300}{137}y_{n+4} + \frac{300}{137}y_{n+3} - \frac{200}{137}y_{n+2} + \frac{75}{137}y_{n+1} - \frac{12}{137}y_n = \frac{60}{137}hf(t_{n+5}, y_{n+5})$

Chapter 4

Validation of PFR Model coupled catalyst-gas chemistry

In this chapter, we will validate our model simulating a PFR reactor with presence a catalyst bed inside with the reference numerical and experiment results.

4.1 Experiment Description

Delgado et al. [26], conducted experimental and numerical study on three reforming methods, are presented in *section 1.1.3*. Because of the COVID-19 pandemic, we can't conduct own experiments to validate our model, therefore, we use the results of Delgado for validation. In their work, they setup the experiment following below:

4.1.1 Equipment Setup

Delgado et al. used a plug flow reactor is shown in Figure 4.1. the reactor is a quartz tube with an inner diameter of 10 mm filled with 20 mg of a Nickel catalyst

with a reaction zone of 27 mm length. The particle size of catalyst is between $500 - 1000\,\mu m$, synthesized by BASF. The porosity of catalytic bed is $\varepsilon_{cat} = 0.42$; the active catalytic area to volume ratio $a_v = 9.85 \times 10^6\ m^{-1}$; and the surface-site density $\Gamma = 2.66 \times 10^{-5}\ mol \cdot m^{-2}$. The dosage of the gases (H_2, CO, O_2, CH_4, CO_2, and N_2) is controlled by mass flow controllers, the water reservoir is controlled by a liquid flow controller. Table 4.1 is summary of experimental equipment.

Table 4.1: Parameters of the experiment

Inner Diameter	Reacting Length	Porosity of Catalytic Bed	Ratio of Active Catalytic Area to Volume	Surface-Site Density
$d\ (mm)$	$L\ (mm)$	ε_{cat}	$a_v\ (m^{-1})$	$\Gamma\ (mol/m^2)$
10	27	0.42	9.85×10^6	2.66×10^{-5}

The volume of reactor is,

$$V_r = \pi \frac{d^2}{4} L = \pi \frac{\left(10 \times 10^{-3}\right)^2}{4} \left(27 \times 10^{-3}\right) = 2.12 \times 10^{-6}\ (m^3)$$

The empty volume in which the gas species flow is,

$$V = \varepsilon_{cat} \cdot V_r = 0.42 \cdot 2.12 \times 10^{-6} = 8.9 \times 10^{-7}\ (m^3)$$

The total active surface of catalyst is,

$$A = V \cdot a_v = 8.9 \times 10^{-7} \cdot 9.85 \times 10^6 = 8.77\ (m^2)$$

4.1.2 Gas Mixture

The gas mixture flow rate at inlet used for all experiment is 4 $slpm$ (standard liters per minute, at 298.15 K temperature and 1.02325 bar pressure) under 1 bar total pressure. The composition of gas mixture for each case study is shown in Table 4.2, N_2 is used to dilute mixture.

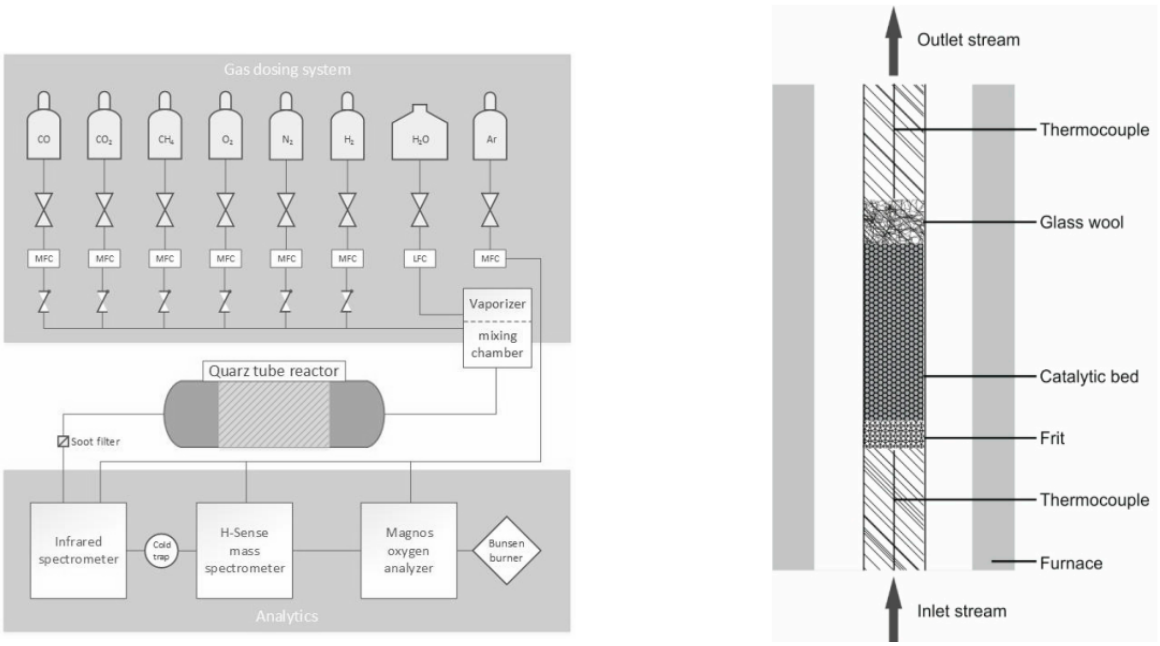

(a) (b)

Figure 4.1: Experiment description. (a) Schematic diagram of the experimental setup used; (b) Schematic diagram of the fixed bed reactor. Source: Delgado et al. from *Catalysts*, 2015.

Table 4.2: Composition of inlet flow for each case study

Case Study	Composition	CH_4 (vol. %)	O_2 (vol. %)	CO_2 (vol. %)	H_2O (vol. %)	N_2 (vol. %)
Steam Reforming	CH_4 / H_2O	1.60	-	-	2.00	96.40
Partial Oxidation	CH_4 / O_2	1.33	0.81	-	-	97.86
Dry Reforming	CH_4 / CO_2	2.00	-	2.00	-	96.00

4.2 Reactor Modeling

4.2.1 Model Description

For simulations *Delgado et al.* used the computer code DETCHEM-PackedBed of the software DETCHEM, which uses an 1D heterogeneous with the assumptions: no radial variations in the flow properties, no axial diffusion, and isothermal operating condition. The governing equations of this 1D model are following below:

- Continuity Equation

$$\frac{d(\rho u)}{dz} = a_v \sum_{i=1}^{K_g} \dot{s}_i M_i$$

- Species Conservation

$$\rho u \frac{d(Y_i)}{dz} + Y_i a_v \sum_{i=1}^{K_g} \dot{s}_i M_i = M_i (a_v \dot{s}_i + \dot{\omega}_i \varepsilon)$$

- Equation of state

$$pM = \rho RT$$

Here, ρ is density; u is velocity; a_v is catalytic area to volume ratio; ε is porosity.

For our simulation, with the same assumptions: *no radial variation, no axial diffusion*, it is completely possible *to model 1D heterogeneous reactor via heterogeneous zero-dimensional reactors*, see Figure 4.2. Because of the neglecting of diffusion, downstream parts of the reactor have no influence on upstream parts. The Plug-Flow Reactor is spatially discretized into a large number of axially distributed volumes. These volumes are modeled to be *steady-state CSTRs*, as presented in *chapter 3*.

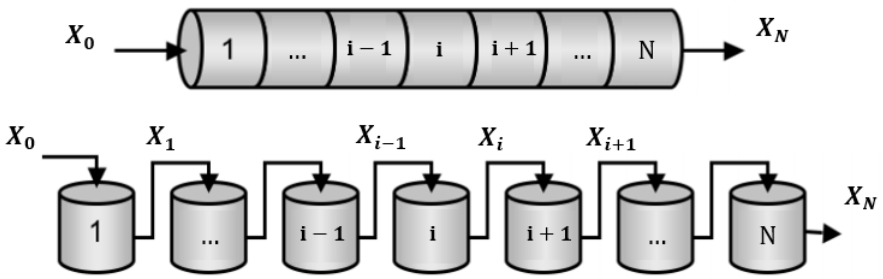

Figure 4.2: Model of PFR reactor by a series of CSTRs reactor

With given state vector X_0 (density, mass fraction, etc.) at inlet of PFR reactor, that will be inlet of first 0D reactor. The state vector X_1 at outlet of first 0D reactor will be the inlet of second 0D reactor. Consequently, the outlet of reactor $(i-1)$, X_{i-1}, is the inlet of reactor i. Finally, the variable vector X_N of 0D reactor N, is the outlet of PFR

reactor.

4.2.2 Equations solved

The transient conservation equations for one heterogeneous 0D reactor having the volume V, and the active area of catalyst A, were presented in *section 3.2*,

- Mass Conservation (Eq. 3.6)

$$\frac{d}{dt}(\rho V) = \dot{m}^* - \dot{m} + \sum_{k=1}^{K_g} \dot{s}_k W_k A$$

- Gas-phase Species Conservation (Eq. 3.9)

$$\rho V \frac{\partial Y_k}{\partial t} = \dot{m}^*(Y_k^* - Y_k) - Y_k\Big(\sum_{j=1}^{K_g} \dot{s}_j W_j A\Big) + \dot{s}_k W_k A + \dot{\omega}_k W_k V \quad \text{for} \quad k = 1..K_g$$

- Surface Species Conservation (Eq. 3.13)

$$\frac{\partial Z_k}{\partial t} = \sigma_k \frac{\dot{s}_k}{\Gamma} \quad \text{for} \quad k = 1..K_s$$

- Energy Conservation (Eq. 3.19)

$$\rho V \bar{c}_p \frac{\partial T}{\partial t} = \dot{m}^* \sum_{k=1}^{K_g} Y_k^*(h_k^* - h_k) - V \sum_{k=1}^{K_g} \dot{\omega}_k W_k h_k - A \sum_{k=1}^{K_g+K_s} \dot{s}_k W_k h_k - \dot{Q} + \dot{P}_d$$

For the steady-state problems and isothermal, we neglect the temporal terms in the conservation equations as well as neglect the energy conservation equation.

- Mass Conservation (Eq. 3.6)

$$0 = \dot{m}^* - \dot{m} + \sum_{k=1}^{K_g} \dot{s}_k W_k A$$

- Gas-phase Species Conservation (Eq. 3.9)

$$0 = \dot{m}^*(Y_k^* - Y_k) - Y_k\Big(\sum_{j=1}^{K_g} \dot{s}_j W_j A\Big) + \dot{s}_k W_k A + \dot{\omega}_k W_k V \quad \text{for} \quad k = 1..K_g$$

- Surface Species Conservation (Eq. 3.13)

$$0 = \sigma_k \frac{\dot{s}_k}{\Gamma} \quad \text{for} \quad k = 1..K_s$$

4.2.3 Numerical Procedure

We solve consequently the state vector of each 0D reactor from the first one to the last one by N times solving the steady-state problem of one heterogeneous 0D reactor.

Despite of the steady-state problem, Cantera still use the transient form of governing equations and **CVODE** solver to give the temporal revolution of the quantities inside reactor for each time-step. Then, it determines the steady-state solution if the residual of the state vector is below a given threshold value. The residual is computed using feature scaling.

$$r = \left| \frac{x(t + \Delta t) - x(t)}{\max(x) + \text{atol}} \right| \cdot \frac{1}{\sqrt{n_x}} \tag{4.1}$$

where, $atol$ is the absolute error tolerance, n_x is maximum number of steps to be taken.

4.2.4 Overview of chemical reactions

Surface Reaction Mechanism

Delgado et al. proposed a surface reactions mechanism consits of 52 elementary step reactions with 14 surface species and 6 gas-phase species, are shown in Table 4.3. The rate coefficients are given in the Arrhenius form $k = AT^B e^{-E_a/RT}$, see detail in *section 2.3.2*.

Table 4.3: Surface reaction mechanism over Nickel catalyst.

Number	Reaction	A $(cm^2/mol\,s)$	B	E_a (kJ/mol)	E_k (kJ/mol)
R1	$H_2 + Ni(s) + Ni(s) \longrightarrow H(s) + H(s)$	3.00×10^{-2}	0.000	5.0	-
R2	$H(s) + H(s) \longrightarrow H_2 + Ni(s) + Ni(s)$	$2.54 \times 10^{+20}$	0.000	95.2	-
R3	$O_2 + Ni(s) + Ni(s) \longrightarrow O(s) + O(s)$	4.36×10^{-2}	-0.206	1.5	-
R4	$O(s) + O(s) \longrightarrow O_2 + Ni(s) + Ni(s)$	$1.18 \times 10^{+21}$	0.823	468.9	-
R5	$H_2O + Ni(s) \longrightarrow H_2O(s)$	1.00×10^{-1}	0.000	0.0	-
R6	$H_2O(s) \longrightarrow H_2O + Ni(s)$	$3.73 \times 10^{+12}$	0.000	60.7	-
R7	$CO_2 + Ni(s) \longrightarrow CO_2(s)$	7.00×10^{-6}	0.000	0.0	-
R8	$CO_2(s) \longrightarrow CO_2 + Ni(s)$	$6.44 \times 10^{+7}$	0.000	25.9	-
R9	$CO + Ni(s) \longrightarrow CO(s)$	5.00×10^{-1}	0.000	0.0	-
R10	$CO(s) \longrightarrow CO + Ni(s)$	$3.56 \times 10^{+11}$	0.000	111.2	$-50.0\,Z_{CO(s)}$
R11	$CH_4 + Ni(s) \longrightarrow CH_4(s)$	8.00×10^{-3}	0.000	0.0	-
R12	$CH_4(s) \longrightarrow CH_4 + Ni(s)$	$8.70 \times 10^{+15}$	0.000	37.5	-
R13	$CH_4(s) + Ni(s) \longrightarrow CH_3(s) + H(s)$	$1.54 \times 10^{+21}$	0.087	55.8	-
R14	$CH_3(s) + H(s) \longrightarrow CH_4(s) + Ni(s)$	$1.44 \times 10^{+22}$	-0.087	63.4	-
R15	$CH_3(s) + Ni(s) \longrightarrow CH_2(s) + H(s)$	$1.54 \times 10^{+24}$	0.087	98.1	-
R16	$CH_2(s) + H(s) \longrightarrow CH_3(s) + Ni(s)$	$3.09 \times 10^{+23}$	-0.087	57.2	-
R17	$CH_2(s) + Ni(s) \longrightarrow CH(s) + H(s)$	$3.70 \times 10^{+24}$	0.087	95.2	-
R18	$CH(s) + H(s) \longrightarrow CH_2(s) + Ni(s)$	$9.77 \times 10^{+24}$	-0.087	81.0	-
R19	$CH(s) + Ni(s) \longrightarrow C(s) + H(s)$	$9.88 \times 10^{+20}$	0.500	21.9	-
R20	$C(s) + H(s) \longrightarrow CH(s) + Ni(s)$	$1.70 \times 10^{+24}$	-0.500	157.9	-
R21	$CH_4(s) + O(s) \longrightarrow CH_3(s) + OH(s)$	$5.62 \times 10^{+24}$	-0.101	92.7	-
R22	$CH_3(s) + OH(s) \longrightarrow CH_4(s) + O(s)$	$2.98 \times 10^{+22}$	0.101	25.8	-
R23	$CH_3(s) + O(s) \longrightarrow CH_2(s) + OH(s)$	$1.22 \times 10^{+25}$	-0.101	134.6	-
R24	$CH_2(s) + OH(s) \longrightarrow CH_3(s) + O(s)$	$1.39 \times 10^{+21}$	0.101	19.0	-
R25	$CH_2(s) + O(s) \longrightarrow CH(s) + OH(s)$	$1.22 \times 10^{+25}$	-0.101	131.3	-
R26	$CH(s) + OH(s) \longrightarrow CH_2(s) + O(s)$	$4.40 \times 10^{+22}$	0.101	42.4	-
R27	$CH(s) + O(s) \longrightarrow C(s) + OH(s)$	$2.47 \times 10^{+21}$	0.312	57.7	-
R28	$C(s) + OH(s) \longrightarrow CH(s) + O(s)$	$2.43 \times 10^{+21}$	-0.312	118.9	-
R29	$H_2O(s) + Ni(s) \longrightarrow H(s) + OH(s)$	$3.67 \times 10^{+21}$	-0.086	92.9	-
R30	$H(s) + OH(s) \longrightarrow H_2O(s) + Ni(s)$	$1.85 \times 10^{+20}$	0.086	41.5	-
R31	$H(s) + O(s) \longrightarrow OH(s) + Ni(s)$	$3.95 \times 10^{+23}$	-0.188	104.3	-
R32	$OH(s) + Ni(s) \longrightarrow H(s) + O(s)$	$2.25 \times 10^{+20}$	0.188	29.6	-
R33	$OH(s) + OH(s) \longrightarrow H_2O(s) + O(s)$	$2.34 \times 10^{+20}$	0.274	92.3	-
R34	$H_2O(s) + O(s) \longrightarrow OH(s) + OH(s)$	$8.14 \times 10^{+24}$	-0.274	218.4	-
R35	$C(s) + O(s) \longrightarrow CO(s) + Ni(s)$	$3.40 \times 10^{+23}$	0.000	148.1	-
R36	$CO(s) + Ni(s) \longrightarrow C(s) + O(s)$	$1.75 \times 10^{+13}$	0.000	116.2	-
R37	$CO(s) + H(s) \longrightarrow C(s) + OH(s)$	$3.52 \times 10^{+18}$	-0.188	105.4	-
R38	$C(s) + OH(s) \longrightarrow CO(s) + H(s)$	$3.88 \times 10^{+25}$	0.188	62.5	$-50.0\,Z_{CO(s)}$

Table 4.3 *Cont.*

Number	Reaction	A $(cm^2/mol\,s)$	B	E_a (kJ/mol)	E_k (kJ/mol)
R39	$CO(s) + CO(s) \longrightarrow C(s) + CO_2(s)$	$1.62 \times 10^{+14}$	0.500	241.7	$-50.0\,Z_{CO(s)}$
R40	$C(s) + CO_2(s) \longrightarrow CO(s) + CO(s)$	$7.29 \times 10^{+28}$	-0.500	239.2	$-100.0\,Z_{CO(s)}$
R41	$CO(s) + O(s) \longrightarrow CO_2(s) + Ni(s)$	$2.00 \times 10^{+19}$	0.000	123.6	-
R42	$CO_2(s) + Ni(s) \longrightarrow CO(s) + O(s)$	$4.64 \times 10^{+23}$	-1.000	89.3	$-50.0\,Z_{CO(s)}$
R43	$CO(s) + OH(s) \longrightarrow COOH(s) + Ni(s)$	$6.00 \times 10^{+21}$	0.213	97.6	-
R44	$COOH(s) + Ni(s) \longrightarrow CO(s) + OH(s)$	$1.46 \times 10^{+24}$	-0.213	54.3	-
R45	$CO_2(s) + H(s) \longrightarrow COOH(s) + Ni(s)$	$6.25 \times 10^{+24}$	-0.475	117.2	-
R46	$COOH(s) + Ni(s) \longrightarrow CO_2(s) + H(s)$	$3.73 \times 10^{+20}$	0.475	33.6	-
R47	$CO(s) + H(s) \longrightarrow HCO(s) + Ni(s)$	$4.00 \times 10^{+20}$	-1.000	132.2	$-50.0\,Z_{CO(s)}$
R48	$HCO(s) + Ni(s) \longrightarrow CO(s) + H(s)$	$3.71 \times 10^{+21}$	0.000	0.0	-
R49	$HCO(s) + Ni(s) \longrightarrow CH(s) + O(s)$	$3.79 \times 10^{+14}$	0.000	81.9	$+50.0\,Z_{CO(s)}$
R50	$CH(s) + O(s) \longrightarrow HCO(s) + Ni(s)$	$4.59 \times 10^{+20}$	0.000	109.9	-
R51	$H(s) + COOH(s) \longrightarrow HCO(s) + OH(s)$	$6.00 \times 10^{+22}$	-1.163	104.8	-
R52	$HCO(s) + OH(s) \longrightarrow H(s) + COOH(s)$	$2.28 \times 10^{+20}$	0.263	15.9	-

Gas-Phase Reaction Mechanism *Delgado et al.* didn't state any the mechanism of gas-phase, which they used in their model. Therefore, we will use a general gas-phase mechanism GRI-MECH 3.0 [27] consisting of 325 elementary chemical reactions and associated rate coefficient expressions and thermochemical parameters for the 53 species involved in them. This popular mechanism was used and tested by the most of research in combustion and chemistry.

Thermodynamics Data The thermodynamics data of all species are gotten from some reliable sources, e.g., Prof. Burcat's Thermodynamic Data [28], Combustion Research Group UC San Diego [29], NIST Chemistry WebBook (National Institute of Standards and Technology) [30], DETCHEM [22, 31].

4.3 Results

We use 200 heterogeneous 0D reactors in series to model this PFR reactor for all of case study, therefore, each 0D reactor have the empty volume $\Delta V = V/200 = 4.453 \times 10^{-9}$ (m^3), the active surface of catalyst $\Delta A = A/200 = 4.386 \times 10^{-3}$ (m^2).

4.3.1 Case Study 1: Steam Reforming

The computed concentrations of gas-phase species at outlet of reactor as a function of temperature from 1D model of *Delgado et al.* and our model, as well as the experimentally measured are shown in Figure 4.3.

Our results are highly close with the numerical results of *Delgado et al.*. Both models fit well with experimental data for CH_4, H_2 and CO speices, however, there are the error for H_2O and CO_2 species.

4.3.2 Case Study 2: Dry Reforming

The computed concentrations of gas-phase species at outlet of reactor as a function of temperature from 1D model of *Delgado et al.* and our model, as well as the experimentally measured are shown in Figure 4.4.

Our results are highly close with the numerical results of *Delgado et al.*. Both models fit well with experimental data for CH_4, CO_2, H_2 and CO speices, however, there are the error for H_2O species.

4.3.3 Case Study 3: Partial Oxidation

The computed concentrations of gas-phase species at outlet of reactor as a function of temperature from 1D model of *Delgado et al.* and our model, as well as the experimentally measured are shown in Figure 4.5.

Our results are highly close with the experimental results with the temperature under 850 K and there are the error from 850 K to 900 K. There are also the difference with the numerical results of *Delgado et al.*, the reason of this difference is the difference in the gas-phase mechanism. Firstly, the mixture of CH_4 and O_2 are burn total (total oxidation) along the length of reactor. Until O_2 is over at a point along the catalytic bed, and then the dry and steam reforming of methane will occur. The total oxidation process is dominated by the gas-phase mechanism, in our simulation, this process is faster than the reference model, see Figure 4.6, Figure 4.7 and Figure 4.8. It causes the difference between two numerical results. However, our results simulated correctly the trend of reacting processes.

4.4 Summary

Up till now, we have developed a numerical tool that simulates a PFR reactor containing the catalyst inside. We have also validated this tool with the 1D model of commercial software DETCHEM used in work of *Delgado et al.*. In general, our tool is suitable and reliable, thus, we could use it to continue developing for next objective.

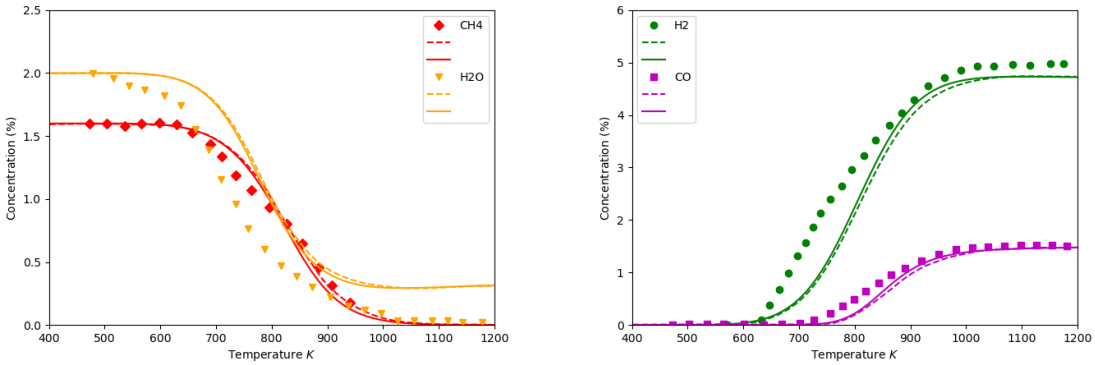

(a) (b)

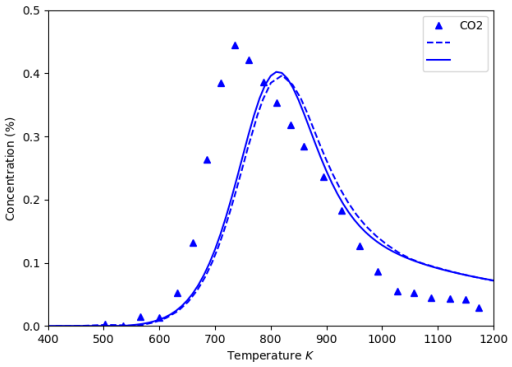

(c)

Figure 4.3: Comparison of experimentally determined (symbols), numerically predicted of *Delgado et al.* (dashed line), and our numerically predicted (solid line) concentrations as a function of temperature for case study of partial oxidation. Inlet gas composition of CH_4 / H_2O = 0.8 in N_2. (a) Concentration of reactants CH_4, H_2O. (b), (c) Concentration of products H_2, CO, and CO_2.

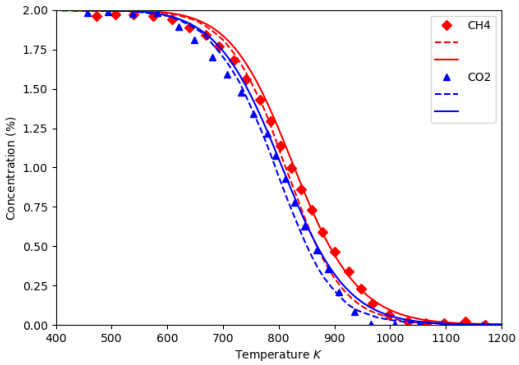

(a)

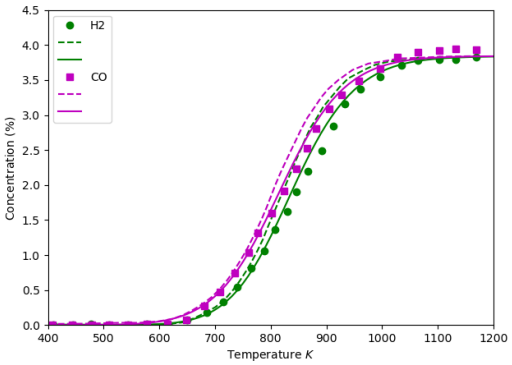

(b)

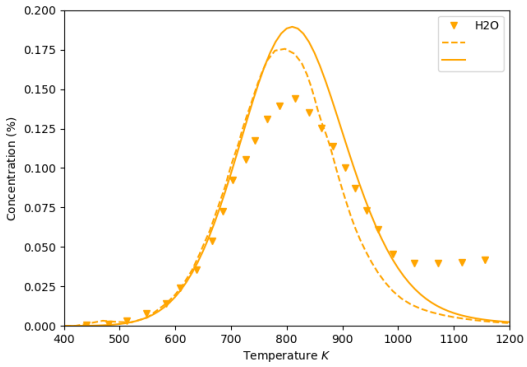

(c)

Figure 4.4: Comparison of experimentally determined (symbols), numerically predicted of *Delgado et al.* (dashed line), and our numerically predicted (solid line) concentrations as a function of temperature for case study of partial oxidation. Inlet gas composition of CH_4 / CO_2 = 1 in N_2. (a) Concentration of reactants CH_4, CO_2. (b), (c) Concentration of products H_2, CO, and H_2O.

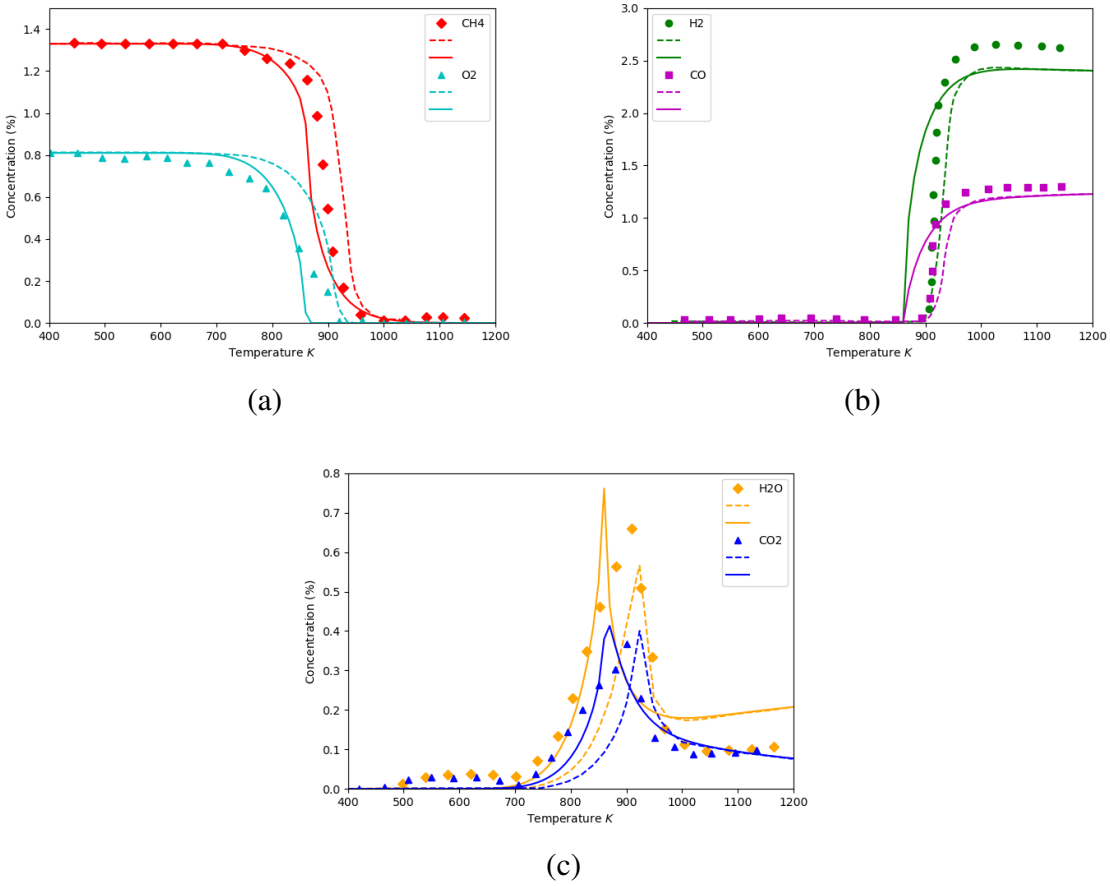

Figure 4.5: Comparison of experimentally determined (symbols), numerically predicted of *Delgado et al.* (dashed line), and our numerically predicted (solid line) concentrations as a function of temperature for case study of partial oxidation. Inlet gas composition of CH_4 / O_2 = 1.6 in N_2. (a) Concentration of reactants CH_4, O_2. (b), (c) Concentration of products H_2, CO, H_2O, and CO_2.

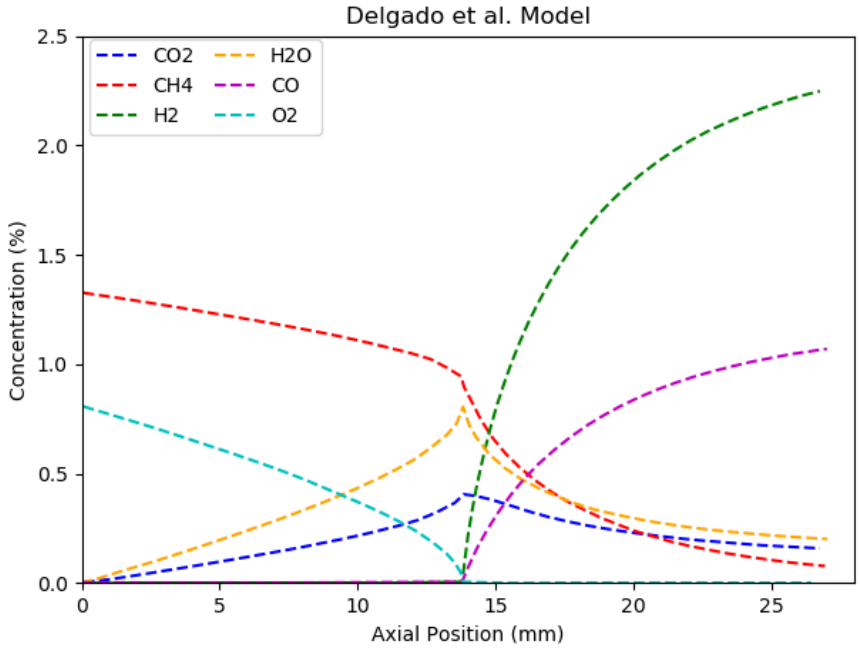

(a) 1D model of *Delgado et al.*

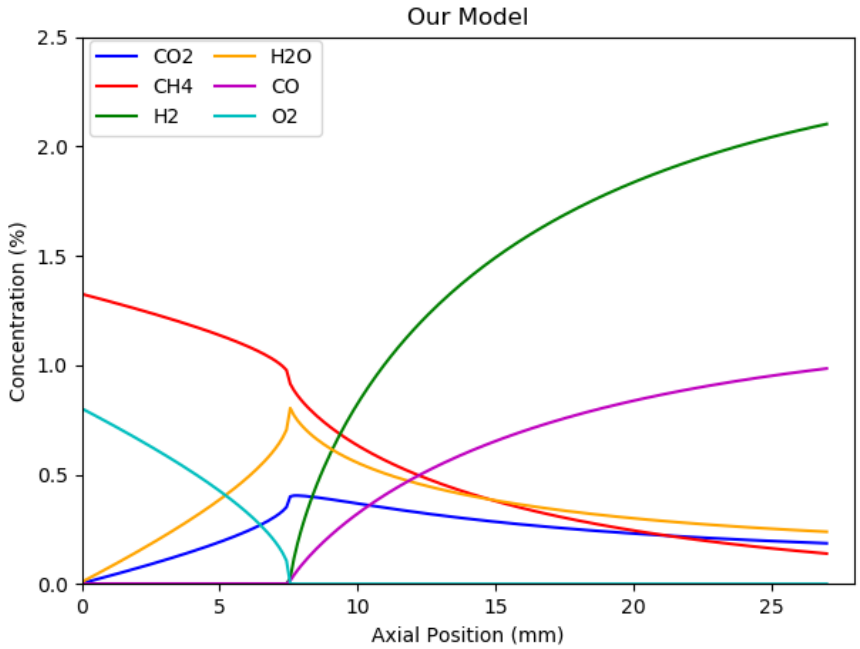

(b) Our Model

Figure 4.6: Gas phase Concentration along the PFR reactor, $T = 973\ K$, CH_4 / O_2 = 1.6, $P = 1\ bar$. (a) computed concentration of *Delgado et al.* as the reference results. (b) our computed concentration

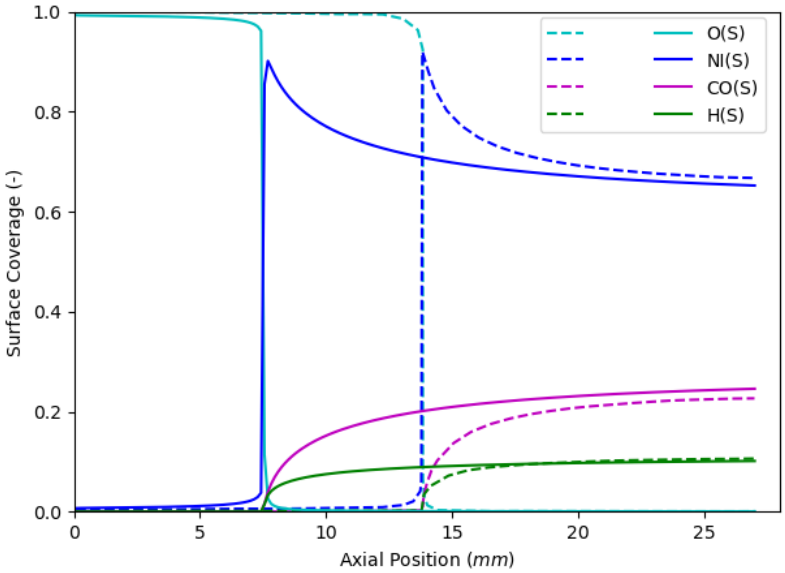

Figure 4.7: Computed surface coverage of O(s), CO(s), H(s), Ni(s). The dashed line is the results of *Delgado et al.* as the reference, and the solid line is our results

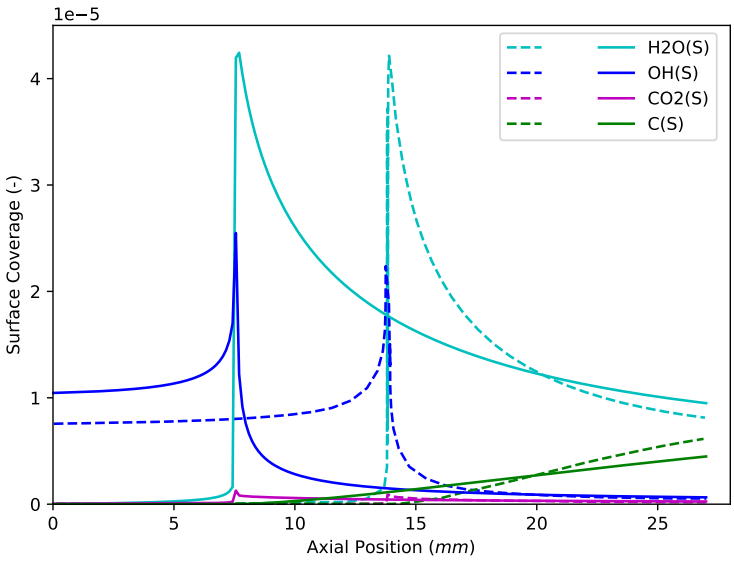

Figure 4.8: Surface Coverage of OH(s), CO_2(s), H_2O(s), C(s). The dashed line is the results of *Delgado et al.* as the reference, and the solid line is our results

Chapter 5

Plasma

In this chapter, the summary of plasma physics will be introduced, as well as the plasma kinetic theory used to study the plasma also will be presented.

5.1 Introduction of Plasma

Plasma is the fourth state of matter, which contains almost the free electron, ion, excited and neutral radicals, molecules. The universe is composed from 99% of plasma, thus, plasma is the biggest state of matter. It can be artificially generated by heating a neutral gas. With enough the applied heating energy, the electrons will exist the electrical clouds to create the charged species, is known as the ion and the free electrons having high energy. In laboratory, the plasma usually is generated by subjecting the neutral gas to a strong electric field. This plasma generating process could be described by following steps below:

1. Under the strong electric field, the electrons will be emitted from the cathode surface, and then be accelerated in the electric field and move forward to the

anode surface.

2. During their mean free path, these electrons ionize the neutral gas by collisions with a heavy particles. Electrons lose only a small portion of its energy while collisions because electrons are much lighter than the heavy particles (That is why the electron temperature in plasma is initially higher than that of heavy particles when using the strong electric field).
3. Subsequently, collisions of electrons with heavy particles (Joule heating) can equilibrate their temperatures.

5.1.1 Properties of plasma

Plasma properties are represented by transport and thermodynamic coefficients often calculated separately and given in tables giving dependence on temperature and pressure.

- **Thermodynamic properties** includes the mass density, the enthalpy, the internal energy, the specific heat, and entropy, which are evaluated for given plasma composition by methods of thermodynamics. The determination of thermodynamics properties is not include in this work.
- **Transport properties** includes the diffusion coefficients, the thermal conductivity, the electrical conductivity, and the viscosity that need for the simulation plasma. Computation of transport coefficients is based on solution of Boltzmann equation. It requires the information of collision cross section for all collisional interactions between particles.

There are three fundamental parameters to characterize a plasma [32]:

- the particle density n (measured in particles per cubic meter)
- the temperature T of each species (usually measured in eV, where $1eV/k_B = 11\,605K$)
- the electric field E (measured in Voltage per meter), and the magnetic field B

(measured in Tesla)

The host of subsidiary parameters (e.g., Debye length, Larmor radius, plasma frequency, cyclotron frequency, thermal velocity) can be derived from these three fundamental parameters. These plasma parameters helps to understand the dynamics of plasma.

5.1.2 Plasma Temperatures: Thermal & Non-Thermal Plasma

Plasma, as multi-component systems, is able to exhibit multiple temperatures, which is divided by two type:

- **Thermal plasma or hot plasma** in which the temperature of electron is the same as the temperature of gas $T_g \approx T_e$, which could be from $5eV$ to some keV.
- **Non-thermal plasma or cold plasma** the electron temperature that often significantly exceeds that of heavy particles, $T_e >> T_g$, temperature of electron can reach some eV. Otherwise, the gas temperature is still close with the ambient temperature. This type of plasma is commonly generated by applying a high voltage into the gas composition.

As in any gas, electron or gas temperature in plasma is determined by the average energies of the particles and their relevant degrees of freedom (translational, rotational, vibrational, and those related to electronic excitation) [33].

5.1.3 Applications of Cold Plasma

The cold plasma requires the low energy input, low operating temperature, it also is easy to install and handling [19]. That was why the cold plasma is being studied for the industrial applications in recent years. For instance,

Production of ozone Ozone is a well-known gaseous chemical agent capable of oxidising a variety of organic and inorganic compounds in gaseous phase, on solid

substrate and aqueous solutions, which is widely used in the agriculture and the food industry. It can remove the pesticides from fruit and vegetable [34]. Werner Siemens, in 1857, proposed his method for reliably generating ozone by passing air or oxygen through an ac discharge bounded by at least one dielectric barrier [35], is known as the generator of non-thermal plasma. Due to ozone

Surface Treatment Cold plasma is used to remove material from surfaces, which can be *chemically selective* and *anisotropic*. *Chemically selective etching* means removing one material and leaving another one unaffected. *Anisotropic etching* involves removing material at the bottom of a trench and leaving the sidewalls unaffected. This method known as plasma etching is one of the key processes applied in microelectronic circuit fabrication. [33].

Biological Decontamination Non-thermal plasma was recently tested for the decontamination of surfaces and liquids (wastewater, ready-to-eat food, food packaging materials), including the inactivation of bacteria, fungi, virus, biomolecules, or biofilm [36]. This application of plasma in medicine is one of the hottest topics.

In the content of this work, the plasma, more specifically, the non-thermal plasma is used to supply the necessary energy for conversion of GHGs without operating at high temperature (over $700°C$).

5.1.4 Chemical Plasma

The chemical plasma reactions are considered as the results of the collisional physical process between the electrons, charged and neutral particles, molecules. There are two type of collisional process [37]:

Primary plasma process – collisions of electrons or electron impact reactions

The physical processes can occur when an electron collides with an atom or molecules, that includes:

- Ionization $\quad e + M \longrightarrow M^+ + 2\,e$
- Dissociative Ionization $\quad e + AB \longrightarrow A^+ + B + 2\,e$
- Electron Attachment $\quad e + M \longrightarrow M^-$
- Dissocitive Electron Attachment $\quad e + AB \longrightarrow A^- + B$
- Excitation $\quad e + M \longrightarrow M^* + e$
- Dissociation $\quad e + AB \longrightarrow A + B$

Elementary reaction rates are determined by the micro-kinetic characteristics of individual reactive collisions being **reaction cross sections** or elementary reaction probabilities, as well as by the kinetic energy of the electron for the particular process. It means that the dependence on how many electrons have enough energy to do the job. It can be described by means of the **electron energy distribution function (EEDF)** $f(\varepsilon)$, which is the probability density for an electron to have energy ε [33].

Secondary plasma process – collisions of heavy particles

The atoms and molecules formed from primary become the reactant in the next stage of the plasma chemistry. These species that involve the excited states, are more active than the original gas and gives rise to large reaction rates. For example:

$$A^- + B^+ \longrightarrow AB$$

$$A^* + B \longrightarrow AB$$

...

5.2 Experiment Description

Let's consider an available experiment set up at IC2MP laboratory, Poitier University [38] is used to study experimentally our subject.

5.2.1 Reactor

A cylindrical alumina tube with a length of $l = 414\ mm$, the external diameter of $d_{ext} = 6\ mm$, the internal diamete of $d_{int} = 4\ mm$, the wall thickness of $1\ mm$. The high voltage electrode is a stainless steel rod with a diameter of $d_{HT} = 1\ mm$, see Figure 5.1a.

5.2.2 Electric Part

To generate a non-thermal plasma, it is necessary to apply a large potential difference between the terminals of two electrodes. The shape of the signal can be impulse, or sinusoidal. In our experiment at IC2MP Lab, only a sinusoidal signal was used to perform the plasma discharge. To do that, a low frequency generator from TTi model TG1010A was coupled to a signal amplifier from TREK model 30/20A. The signal delivered by the low frequency generator can be sinusoidal, square or even triangular. The amplifier increases the value of the voltage supplied by the low frequency generator (x3000 peak to peak), thus making it possible to work at high voltages, see Figure 5.1b

5.3 Non-Thermal Plasma Modeling

As presented in previous section, plasma is defined a gas of charged and neutral particles. Therefore, in order to take into account the affects of plasma to a 0D reactor model, we can consider the plasma is a set of new species in the reactor model. It means that the reactor model will be added new species e.g., electron, position ions, negative ions, neutral particles considered as the gas-phase species, as well as the reactor will have not only the homogeneous reactions and the heterogeneous reactions, but also the plasma chemical reactions (electron-impact reactions).

In non-thermal plasma, the temperature difference between electrons and other species

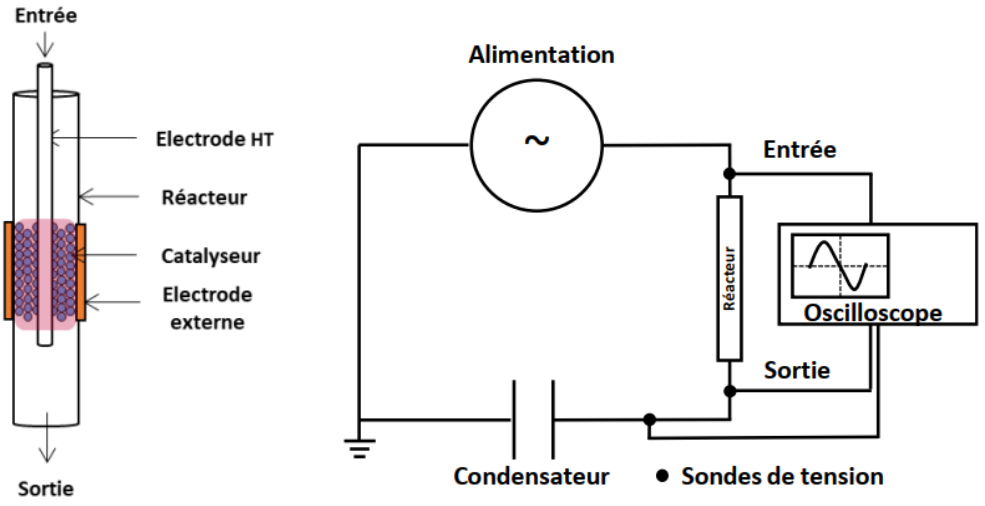

(a) (b)

Figure 5.1: Experiment description (a) Schema of reactor set up at IC2MP Lab, (b) Schema of electric circuit used in experiment. Source: Ph.D Thesis of Nassim BOUCHOUL, *Valorisation du dioxyde de carbone par couplage plasma non-thermique et catalyse*, Poitier University, 2019.

cause the change of energy conservation equation modeling a plasma-assisted reactor, which leads to a two-temperature model. However, in this content of this work, we just take a look the final equations used in commercial software CHEMKIN [20, 21], and don't discuss on proofing it.

Bulk energy conservation or total energy conservation, is used to determined the temperature of gas. It is similar with the total energy conservation from equation (3.19), which separate the enthalpy of electrons into a term due to the difference of temperature.

$$\begin{aligned}\rho V \bar{c}_p \frac{\partial T}{\partial t} + \rho V Y_e \frac{5}{2}\frac{k_B}{W_e}\frac{\partial T_e}{\partial t} = \dot{m}^* \sum_{k=1}^{K_g} Y_k^*(h_k^* - h_k) - V \sum_{k=1}^{K_g} \dot{\omega}_k W_k h_k \\ - A \sum_{k=1}^{K_g+K_s} \dot{s}_k W_k h_k - \dot{Q} + \dot{P}_d\end{aligned} \tag{5.1}$$

Where k_B is Boltzmann constant, and W_e is molecular weight of electron.

Electron energy conservation, is used to determined the electron temperature. The

rate of change if the electron internal energy, u_e, equals the net flow of electron enthalpy into and out of reactor, accounting for net chemical production rates, surface losses, collisions losses, and power deposition from externally applied electromagnetic fields.

$$\begin{aligned}\frac{3}{2}\frac{k_B}{W_e}\rho V Y_e\frac{\partial T_e}{\partial t} = &\frac{5}{2}\frac{k_B}{W_e}\dot{m}^* Y_e\left(T_e^* - T_e\right) + \frac{k_B}{W_e}\dot{m}^* T_e\left(Y_e^* - Y_e\right)\\ &- \frac{k_B}{W_e}T_e Y_e A\sum_{k=1}^{K_g}\dot{s}_k W_k + \frac{k_B}{W_e}T_e\left(\dot{s}_e W_e A + \dot{\omega}_e W_e V\right)\\ &+ \frac{5}{2}\frac{k_B}{W_e}\dot{\omega}_e W_e V\left(T - T_e\right) - Q_{elas} - Q_{inel} + \dot{P}_d^{'}\end{aligned} \tag{5.2}$$

In equation (5.2), the first three terms on the right hand side accounts for the difference in inlet and outlet enthalpy of electrons. The fourth term represents the net production of electron enthalpy through both heterogeneous and homogeneous gas-phase reactions. The fifth term accounts for the energy of electron required to thermalize newly produced electrons. Q_{elas}, Q_{inel} are elastic and inelastic energy loss terms, respectively (determination of these terms will be presented in *section 6.7).* $\dot{P}_d^{'}$ is the net power deposited to electrons taking into the power transferred to the ions.

$$\dot{P}_d^{'} = \dot{P}_d - a_{sh}\sum_{ions}\dot{s}_i A k_B T_e - \sum_{ions}\dot{\omega}_i V k_B(T_{ion} - T)$$

Where, a_{sh} is a multiplier of the electron energy $(k_B T_e)$ used to describe the energy gained by ions as they traverse the sheath and before they recombine on a surface.

We can see that in order to take into account the plasma to the reactor model, first of all, it is necessary the determination the relevant plasma coefficient presenting in the fluid description equations above, e.g., Q_{elas}, Q_{inel}, and the rate of progress of each electron-impact reaction. That is why we still not discuss deeply about the two-temperature model which will be used for our model in the future and this problem will be studied later.

5.4 Plasma Kinetic Theory

The plasma coefficients is relevant to the plasma chemical reaction being the results of micro-kinetic in plasma. However, If we study plasma in the microscope that means we track the motion of individual particles, there will be a huge calculation. It is actually impossible to solve despite of having the strong support of computer. So, a statistical approach is more reliable, is known as Plasma kinetic theory. Plasma kinetic theory presented in this section is a part of lecture notes of *Prof. John Howard* [39] in the field of plasma physics at the Australian National University.

5.4.1 Distribution Function

The centre of kinetic theory is the distribution function $f(\boldsymbol{r}, \boldsymbol{v}, t)$, if we obtain the distribution function, all the information about plasma can be known. There are 7 independence variables in the distribution function: 3 position variables $\boldsymbol{r}$, 3 velocity variables $\boldsymbol{v}$ and time t.

$$\boldsymbol{r} = x\hat{\boldsymbol{i}} + y\hat{\boldsymbol{j}} + z\hat{\boldsymbol{k}} \tag{5.3}$$

$$\boldsymbol{v} = v_x\hat{\boldsymbol{i}} + v_y\hat{\boldsymbol{j}} + v_z\hat{\boldsymbol{k}} \tag{5.4}$$

The coordinates $(\boldsymbol{r}, \boldsymbol{v})$ is called *phase-space* defining the state of particle. The distribution function defined is the number of particles at time t in the element of volume $dV = d\boldsymbol{v}d\boldsymbol{r}$ in phase space.

$$f(\boldsymbol{r}, \boldsymbol{v}, t)d\boldsymbol{r}d\boldsymbol{v} = dN(\boldsymbol{r}, \boldsymbol{v}, t) \tag{5.5}$$

Here, $d\boldsymbol{r} \equiv d^3r \equiv dxdydz$ and $d\boldsymbol{v} \equiv d^3v \equiv dv_xdv_ydv_z$. The distribution function is a positive finite function that decreases to zero as $|\boldsymbol{v}|$ becomes large.

5.4.2 Boltzmann Equation

The Boltzmann equation describes the time evolution of f under the action of external forces and internal collisions. $f(\boldsymbol{r}, \boldsymbol{v}, t)$ changes because of the flux of particles across the surface bounding the elemental volume $(d\boldsymbol{r}d\boldsymbol{v})$ in phase space. This can arise continuously due to particle velocity and external forces (accelerations) or discontinuously through collisions. The collisional contribution to the rate of change $\partial f/\partial t$ of the distribution function is written as $(\partial f/\partial t)_{coll}$.

We let $\boldsymbol{V} = (\boldsymbol{v}, \boldsymbol{a})$ be the generalized "velocity" vector for our mathematical phase space $(\boldsymbol{r}, \boldsymbol{v})$, then the rate of flow over S into the volume element is

$$-\int_S (\boldsymbol{V}f)\, d\boldsymbol{s} \tag{5.6}$$

Here $\boldsymbol{V}f$ is the definition of particle flux.

Then, using the divergence theorem, the rate of flow (Eq. 5.6) can be written

$$-\int_{\Delta V} d\boldsymbol{r}d\boldsymbol{v}\, [\nabla_r(\boldsymbol{v}f) + \nabla_v(\boldsymbol{a}f)] \tag{5.7}$$

Where, ∇_r is the divergence with respect to $\boldsymbol{r}$ and ∇_v is the divergence operator with respect to $\boldsymbol{v}$.

$$\nabla_r \equiv \frac{\partial}{\partial x}\hat{\boldsymbol{i}} + \frac{\partial}{\partial y}\hat{\boldsymbol{j}} + \frac{\partial}{\partial z}\hat{\boldsymbol{k}}$$

$$\nabla_v \equiv \frac{\partial}{\partial v_x}\hat{\boldsymbol{i}} + \frac{\partial}{\partial v_y}\hat{\boldsymbol{j}} + \frac{\partial}{\partial v_z}\hat{\boldsymbol{k}}$$

The inclusion of the continuous phase space flow term and the discontinuous collision term then gives the result

$$\int_{\Delta V} \frac{\partial f}{\partial t} d\boldsymbol{r}d\boldsymbol{v} = -\int_{\Delta V} d\boldsymbol{r}d\boldsymbol{v}\, [\nabla_r(\boldsymbol{v}f) + \nabla_v(\boldsymbol{a}f)] + \int_{\Delta V} \left(\frac{\partial f}{\partial t}\right)_{coll} d\boldsymbol{r}d\boldsymbol{v} \tag{5.8}$$

Or in differential form

$$\frac{\partial f}{\partial t} = -\nabla_r(\boldsymbol{v} f) - \nabla_v(\boldsymbol{a} f) + \left(\frac{\partial f}{\partial t}\right)_{coll} \tag{5.9}$$

The acceleration can be written in terms of the force $\boldsymbol{F} = m\boldsymbol{a}$ applied or acting on the particle species. For plasma, the dominant force is electromagnetic, the Lorentz force

$$\boldsymbol{F} = q\left(\boldsymbol{E} + \boldsymbol{v} \times \boldsymbol{B}\right) \equiv m\boldsymbol{a} \tag{5.10}$$

Using the vector identity (product rule)

$$\nabla(a\boldsymbol{A}) = \boldsymbol{A}\nabla a + a\nabla\boldsymbol{A}$$

Moreover, since $\boldsymbol{r}$ and $\boldsymbol{v}$ are independent coordinates, we finally obtain the *Boltzmann equation (BE)*

$$\frac{\partial f}{\partial t} + \boldsymbol{v} \cdot \nabla_r f + \frac{q}{m}\left(\boldsymbol{E} + \boldsymbol{v} \times \boldsymbol{B}\right) \cdot \nabla_v f = \left(\frac{\partial f}{\partial t}\right)_{coll} \tag{5.11}$$

Applying the Boltzmann equation to our study, a non-thermal plasma only generated by strong electric field ($\boldsymbol{B} = 0$), thus the Boltzmann equation of electron is

$$\frac{\partial f}{\partial t} + \boldsymbol{v} \cdot \nabla_r f - \frac{e}{m}\boldsymbol{E} \cdot \nabla_v f = \left(\frac{\partial f}{\partial t}\right)_{coll} \tag{5.12}$$

Chapter 6

Boltzmann Equation Solver

We will discuss a numerical method for solving the Boltzmann equation in this chapter. The results of our BE solver developed in Python environment also is compared with the common BE solver - BOLSIG+.

The electrons distribution function can be calculated using standard programs such as ELENDIF (Morgan and Penetrante, 1990) [40] and BOLSIG+ (Hagelaar and Pitchford, 2005) [41] and is related to the electron temperature in a look-up table. Usually, in order to conduct a simulation of plasma-assisted reactor, we have to use two separated modules: one is Boltzmann equation solver, and another is reactor model. The data of plasma from BE solver are inputted into reactor model and then are linearized while modeling, this take us a lot of time to conduct. So, it requires a BE solver in Python environment to make the sync of whole our simulation tool.

In this section, we will discuss the numerical method solving BE of *Hagelaar and Pitchford*, which used in BOLSIG+, then, use it in our study.

In order to solve the BE, we need to make some simplifications. We limit to the case where the electric filed and the collision probabilities are all spatially uniform.

The electron distribution f is symmetric in velocity space around the electric field direction. In position space, f may vary along the field direction. Finally, using spherical coordinates in velocity space, we obtain

$$\frac{\partial f}{\partial t} + v\cos\theta\frac{\partial f}{\partial z} - \frac{e}{m}E\left(\cos\theta\frac{\partial f}{\partial v} + \frac{\sin\theta^2}{v}\frac{\partial f}{\partial\cos\theta}\right) = \left(\frac{\partial f}{\partial t}\right)_{coll} \equiv C[f] \tag{6.1}$$

Here $C[f]$ is collision term.

6.1 Two-term approximation

A common approach to solve equation (6.1) is to expand f in terms of Legendre polynomials of $\cos\theta$ (spherical harmonics expansion) and then construct from equation (6.1) a set of equations for the expansion coefficients. Using the two-term approximation we expand f as

$$f(v,\cos\theta,z,t) = \sum_{n=0}^{1} f_n P_n(\cos\theta) = f_0(v,z,t) + f_1(v,z,t)\cos\theta \tag{6.2}$$

where, $P_n(\cos\theta)$ is Legendre polynomials ($P_0(\cos\theta) = 1, P_1(\cos\theta) = \cos\theta$), f_0 is the isotropic part of f and f_1 is an anisotropic perturbation.

Equation (6.1) by substituting equation (6.2), multiplying by the respective Legendre polynomials (1 and $\cos\theta$) and integrating over $\cos\theta$, leads to the hierarchy of coupled partial differential equations [42]:

$$\frac{\partial f_0}{\partial t} + \frac{\gamma}{3}\varepsilon^{1/2}\frac{\partial f_1}{\partial z} - \frac{\gamma}{3}\varepsilon^{-1/2}\frac{\partial}{\partial\varepsilon}(\varepsilon E f_1) = C_0 \tag{6.3}$$

$$\frac{\partial f_1}{\partial t} + \gamma\varepsilon^{1/2}\frac{\partial f_0}{\partial z} - E\gamma\varepsilon^{1/2}\frac{\partial f_0}{\partial\varepsilon} = -N\sigma_m\gamma\varepsilon^{1/2}f_1 \tag{6.4}$$

where $\gamma = (2e/m)^{1/2}$ is a constant and $\varepsilon = (v/\gamma)^2$ is the electron energy in electronvolts. The right-hand side of equation (6.3) represents the change in f_0 due to

collisions. The right hand side of equation (6.4) contains the total momentum-transfer cross-section σ_m consisting of contributions from all possible collision processes k with gas particles.

$$\sigma_m = \sum_k X_k \sigma_k \tag{6.5}$$

where X_k is the mole fraction of the target species of the collision process. σ_k is cross section gotten from database LXCat [43].

6.2 Growth of the electron density

By making assumptions about the temporal and spatial dependence of f_0 and f_1, we separate the energy-dependence of f from its dependence on time and space by assuming that

$$f_{0,1}(\varepsilon, z, t) = \frac{1}{2\pi\gamma^3} F_{0,1}(\varepsilon) n(z, t) \tag{6.6}$$

where the energy distribution $F_{0,1}$ is constant in time and space and normalized by

$$\int_0^\infty \varepsilon^{1/2} F_0 d\varepsilon = 1 \tag{6.7}$$

The time or space dependence of the electron density n is now related to the net electron production rate. For this, we consider two simple cases corresponding to specific swarm experiments. Most discharges resemble at least one of these cases

6.2.1 Exponential temporal growth without space dependence

This case corresponds to Pulsed Townsend experiments. The temporal growth rate of the electron number density equals the net production frequency $\bar{\nu}_i$.

$$\frac{1}{n}\frac{\partial n}{\partial t} = \bar{\nu}_i \equiv N\gamma \int_0^\infty \left(\sum_{k=ionization} X_k \sigma_k - \sum_{k=attachment} X_k \sigma_k \right) \times \varepsilon F_0 d\varepsilon \tag{6.8}$$

Here, n is the electron density and N is the gas density.

Equation (6.4) becomes

$$F_1 = \frac{E}{N}\frac{1}{\tilde{\sigma}_m}\frac{\partial F_0}{\partial \varepsilon} \tag{6.9}$$

Substituting this in equation (6.3), we obtain

$$-\frac{\gamma}{3}\frac{\partial}{\partial \varepsilon}\left(\left(\frac{E}{N}\right)^2 \frac{\varepsilon}{\tilde{\sigma}_m}\frac{\partial F_0}{\partial \varepsilon}\right) = \tilde{C}_0 + \tilde{R} \tag{6.10}$$

Where,

$$\tilde{\sigma}_m = \sigma_m + \frac{\bar{\nu}_i}{N\gamma\varepsilon^{1/2}}$$

$$\tilde{R} = -\frac{\bar{\nu}_i}{N}\varepsilon^{1/2}F_0$$

6.2.2 Exponential spatial growth without time dependence

This case corresponds to Steady State Townsend experiments. The density grow exponentially with a constant spatial growth rate α (Townsend coefficient), which is related to the net electron production by

$$\alpha \equiv -\frac{1}{n}\frac{\partial n}{\partial z} = -\frac{\bar{\nu}_i}{w} \tag{6.11}$$

where the mean velocity w is determined by F_1, constant in space and negative. Using the definition of α, equation (6.4) becomes

$$F_1 = \frac{1}{\sigma_m}\left(\frac{E}{N}\frac{\partial F_0}{\partial \varepsilon} + \frac{\alpha}{N}F_0\right) \tag{6.12}$$

Equation (6.3) can again be written in the form

$$-\frac{\gamma}{3}\frac{\partial}{\partial \varepsilon}\left(\left(\frac{E}{N}\right)^2 \frac{\varepsilon}{\tilde{\sigma}_m}\frac{\partial F_0}{\partial \varepsilon}\right) = \tilde{C}_0 + \tilde{R} \tag{6.13}$$

Where,

$$\tilde{\sigma}_m = \sigma_m$$

$$\tilde{R} = \frac{\alpha}{N}\frac{\gamma}{3}\left[\frac{\varepsilon}{\sigma_m}\left(2\frac{E}{N}\frac{\partial F_0}{\partial \varepsilon} + \frac{\alpha}{N}F_0\right) + \frac{E}{N}F_0\frac{\partial}{\partial \varepsilon}\left(\frac{\varepsilon}{\sigma_m}\right)\right]$$

6.3 Oscillating Field

Now we consider the oscillating electric field having the complex notation is

$$E(t) = E_0 e^{i\omega t} \tag{6.14}$$

Using the two-term approximation:

$$f(v, \cos\theta, z, t) = f_0(v, z, t) + f_1(v, z, t)\cos\theta e^{i\omega t} \tag{6.15}$$

where the time-variation of f_0 and f_1 is slow with respect to the oscillation; f_1 may be complex to account for phase shifts with respect to the electric field.

Using equation (6.15), we proceed exactly as before. Only the temporal growth model makes sense, because the oscillating field does not lead to time-averaged transport, and we obtain

$$F_1 = \frac{E_0}{N}\frac{\tilde{\sigma}_m - iq}{\tilde{\sigma}_m^2 + q^2}\frac{\partial F_0}{\partial \varepsilon} \tag{6.16}$$

Here, $\tilde{\sigma}_m = \sigma_m + \bar{\nu}_i / N\gamma\varepsilon^{1/2}$ and $q = \omega / N\gamma\varepsilon^{1/2}$.Substituting this in the equation for F_0 and averaging the energy absorption over the field cycle, we finally obtain

$$-\frac{\gamma}{3}\frac{\partial}{\partial \varepsilon}\left(\left(\frac{E_0}{N}\right)^2 \frac{\tilde{\sigma}\varepsilon}{2\left(\tilde{\sigma}_m^2 + q^2\right)}\frac{\partial F_0}{\partial \varepsilon}\right) = \tilde{C}_0 + \tilde{R} \tag{6.17}$$

equation (6.17) can be written exactly as equation (6.10) for a stationary electric field,

where the field E is replaced by an effective field

$$E_{eff} = \sqrt{2\left(1 + \omega^2/\nu^2\right)}E_0 \tag{6.18}$$

Where, $\nu = \tilde{\sigma}_m N\gamma\varepsilon^{1/2}$

6.4 Collision Terms

The right-hand side of equations (6.10), (6.13) and (6.17) contain the collision term consisting of contributions from all different collision processes k with neutral gas particles and from electron–electron collisions:

$$\tilde{C}_0 = \sum_k \tilde{C}_{0,k} + \tilde{C}_{0,e} \tag{6.19}$$

Elastic collisions: The effect of elastic collisions can be described by

$$\tilde{C}_{0,k=elastic} = \gamma X_k \frac{2W_e}{W_k}\frac{\partial}{\partial\varepsilon}\left[\varepsilon^2\sigma_k\left(F_0 + \frac{k_B T}{e}\frac{\partial F_0}{\partial\varepsilon}\right)\right] \tag{6.20}$$

where W_k is the molecular weight of the target particles and T is their temperature. The first term represents the kinetic energy lost to the target particles and the second term is the energy gained from the target particles assuming that these are Maxwellian.

Excitation/de-excitation

$$\tilde{C}_{0,k=inelastic} = -\gamma X_k\left[\varepsilon\sigma_k(\varepsilon)F_0(\varepsilon) - (\varepsilon + u_k)\sigma_k(\varepsilon + u_k)F_0(\varepsilon + u_k)\right] \tag{6.21}$$

where u_k is the threshold energy of the collision and is negative for de-excitation. The two terms are known, respectively, as the scattering-out and scattering-in terms; the scattering-in term clearly vanishes for $\varepsilon < -u_k$ in the case of de-excitation.

Ionization: The effect of ionization depends on how the remaining energy is shared

by the two electrons after ionization. Here we consider only the two limiting cases of equal and zero energy sharing.

In the case of equal energy sharing

$$\tilde{C}_{0,k=ionization} = -\gamma X_k \left[\varepsilon\sigma_k(\varepsilon)F_0(\varepsilon) - 2(2\varepsilon + u_k)\sigma_k(2\varepsilon + u_k)F_0(2\varepsilon + u_k)\right] \quad (6.22)$$

In the case of equal energy sharing

$$\begin{aligned}\tilde{C}_{0,k=ionization} = &- \gamma X_k \left[\varepsilon\sigma_k(\varepsilon)F_0(\varepsilon) - (\varepsilon + u_k)\sigma_k(\varepsilon + u_k)F_0(\varepsilon + u_k)\right] \\ &+ \delta(\varepsilon)\gamma X_k \int_0^\infty u\sigma_k(u)F_0(u)du\end{aligned} \quad (6.23)$$

Attachment: Attachment simply removes electrons from the energy distribution

$$\tilde{C}_{0,k=attachment} = -\gamma X_k \varepsilon\sigma_k(\varepsilon)F_0(\varepsilon) \quad (6.24)$$

Electron–electron collisions

$$\tilde{C}_{0,e} = a\frac{n}{N}\frac{\partial}{\partial\varepsilon}\left[3A_1F_0 + 2\left(A_2 + \varepsilon^{3/2}A_3\frac{\partial F_0}{\partial\varepsilon}\right)\right] \quad (6.25)$$

Where,

$$A_1 = \int_0^\varepsilon u^{1/2}F_0(u)du$$

$$A_2 = \int_0^\varepsilon u^{3/2}F_0(u)du$$

$$A_3 = \int_\varepsilon^\infty F_0(u)du$$

$$a = \frac{e^2\gamma}{24\pi\varepsilon_0^2}\ln\Lambda$$

$$\Lambda = \frac{12\pi(\varepsilon_0 k_B T_e)^{3/2}}{e^3 n^{1/2}}$$

$$k_B T_e = \frac{2}{3} e A_2(\infty)$$

6.5 Equation for the EEDF

Combining the previous equations, we find an equation for F_0 that looks like a convection - diffusion continuity equation in energy space

$$\frac{\partial}{\partial \varepsilon}\left(\tilde{W} F_0 - \tilde{D}\frac{\partial F_0}{\partial \varepsilon}\right) = \tilde{S} \tag{6.26}$$

Where

$$\tilde{W} = -\gamma \varepsilon^2 \sigma_\varepsilon - 3a\frac{n}{N} A_1 \tag{6.27}$$

$$\tilde{D} = \frac{\gamma}{3}\left(\frac{E}{N}\right)^2 \frac{\varepsilon}{\tilde{\sigma}_m} + \frac{\gamma k_B T}{e}\varepsilon^2 \sigma_\varepsilon + 2a\frac{n}{N}(A_2 + \varepsilon^{3/2} A_3) \tag{6.28}$$

$$\sigma_\varepsilon = \sum_{k=elastic} \frac{2W_e}{W_k} X_k \sigma_k \tag{6.29}$$

$$\tilde{S} = \sum_{k=inelastic} \tilde{C}_{0,k} \tag{6.30}$$

The left-hand side of equation (6.26) as the divergence of the electron flux in energy space. This flux then has a convection part with a negative flow velocity $\tilde{W}$, representing cooling by elastic collisions with less energetic particles (neutrals or electrons), and a diffusive part with diffusion coefficient $\tilde{D}$, representing heating by the field and by elastic collisions with more energetic particles. The source term $\tilde{S}$ on the right-hand side of equation (6.26) has the special property that it is non-local, it depends on energies elsewhere in energy space. This means that the equation is no ordinary differential equation and solving it requires some special methods.

6.6 Numerical solution of the equation

Equation (6.26) is discretized on a grid in energy space, consisting of a series of subsequent energy intervals, here called grid cells, numbered $i = 1, 2, ...$ The subscript i refers to the centre of the grid cell i and the subscript $i + 1/2$ to the boundary between the cells i and $i + 1$. The energy distribution function F_0 is defined in the cell centres. For each cell i we obtain a linear equation relating the local value $F_{0,i}$ to the values $F_{0,j}$ in the other cells, by integrating the differential equation over the cell:

$$\left[\tilde{W}F_0 - \tilde{D}\frac{\partial F_0}{\partial \varepsilon}\right]_{i+1/2} - \left[\tilde{W}F_0 - \tilde{D}\frac{\partial F_0}{\partial \varepsilon}\right]_{i-1/2} = \int_{\varepsilon_i - 1/2}^{\varepsilon_i + 1/2} \tilde{S} d\varepsilon \tag{6.31}$$

The left-hand side of the equation is discretized by the exponential scheme of Scharfetter and Gummel [44] commonly used for convection-diffusion problems:

$$\left[\tilde{W}F_0 - \tilde{D}\frac{\partial F_0}{\partial \varepsilon}\right]_{i+1/2} = \frac{\tilde{W}_{i+1/2}F_{0,i}}{1 - \exp\left(-z_{i+1/2}\right)} + \frac{\tilde{W}_{i+1/2}F_{0,i+1}}{1 - \exp\left(z_{i+1/2}\right)} \tag{6.32}$$

where $z_{i+1/2} = \tilde{W}_{i+1/2}(\varepsilon_{i+1} - \varepsilon_i)/\tilde{D}_{i+1/2}$ (Peclet number).

The inelastic collision terms on the right-hand side are non-local in energy but linear in F_0 and are evaluated fully implicitly, which involves direct inversion of a matrix that is more or less sparse, depending on the different threshold energies of the collisions. We discretize as follows:

$$\int_{\varepsilon_i - 1/2}^{\varepsilon_i + 1/2} \tilde{S} d\varepsilon \equiv -P_i F_{0,1} + \sum_j Q_{i,j} F_{0,j} \tag{6.33}$$

Where

$$P_i = \sum_{inelastic} \gamma X_k \int_{\varepsilon_{i-1/2}}^{\varepsilon_{i+1/2}} \varepsilon \sigma_k \exp\left[(\varepsilon_i - \varepsilon) g_i\right] d\varepsilon \tag{6.34}$$

$$Q_i = \sum_{inelastic} \gamma X_k \int_{\varepsilon_1}^{\varepsilon_2} \varepsilon \sigma_k \exp\left[(\varepsilon_j - \varepsilon) g_j\right] d\varepsilon \tag{6.35}$$

where the interval $[\varepsilon_1, \varepsilon_2]$ is the overlap of cell j, and cell i shifted by the threshold energy u_k:

$$\varepsilon_1 = \min\left(\max(\varepsilon_{i-1/2} + u_k, \varepsilon_{j-1/2}), \varepsilon_{j+1/2}\right) \tag{6.36}$$

$$\varepsilon_2 = \min\left(\max(\varepsilon_{i+1/2} + u_k, \varepsilon_{j-1/2}), \varepsilon_{j+1/2}\right) \tag{6.37}$$

The exponential factors in the P- and Q-integrals assume the distribution F_0 to be piecewise exponential, with a (local) logarithmic slope estimated as

$$g_i = \frac{1}{\varepsilon_{i+1} - \varepsilon_{i-1}} \ln\left(\frac{F_{0,i+1}}{F_{0,i-1}}\right) \tag{6.38}$$

The discretized equation is implicit, thus, **EEDF** is solved by using the iteration produce.

6.7 Coefficient of Plasma in Fluid Model

The previous sections, we have built a numerical strategy for solving the Boltzmann equation to obtain the electron energy distribution function (**EEDF**). From EEDF, we completely get all information of plasma in the governing equations of plasma-assisted reactor model.

Mean energy (eV)

$$\langle\varepsilon\rangle = \int_0^\infty \varepsilon^{3/2} F_0 d\varepsilon \tag{6.39}$$

Elastic power loss /N $(eV \cdot m^3/s)$

$$\frac{\dot{Q}_{elas}}{N} = \sum_{k=elastic} \gamma X_k \frac{2W_e}{W_k} \int_0^\infty \left[\sigma_k \left(\varepsilon^2 F_0 + \frac{k_B T}{e} \frac{\partial F_0}{\partial \varepsilon}\right)\right] \tag{6.40}$$

Inelastic power loss /N $(eV \cdot m^3/s)$

$$\frac{\dot{Q}_{inel}}{N} = \sum_{k=inelastic} u_k X_k k_k \tag{6.41}$$

u_k is threshold energy of inelastic collision process k.

Electron Impact Reaction Rate coefficients (m^3/s)

$$k_k = \gamma \int_0^\infty \varepsilon \sigma_k F_0 d\varepsilon \tag{6.42}$$

6.8 Results

Our BE solver is built and developed based on the BOLOS [45] library (BOLtzmann equation solver Open Source library) in Python environment. This library was developed by *Alejandro Luque* at the Instituto de Astrofísica de Andalucía (IAA), CSIC. BOLOS follows the algorithm described by *Hagelaar and Pitchford* which we have taken a look in this chapter. However, BOLOS just take into account the constant electric field, $E = const$ while our experiment operates in sinusoidal electric field. Therefore, I developed BOLOS being able to deal with oscillating field as a part of content in this internship.

Let's test the code in the study case shown in Table. 6.1, with the assumptions: exponential temporal growth, oscillating electric field, and only collisions with ground state gas particles. The electron impact reactions are shown in Table 6.2, its cross section data are gotten from PHELPS database [46] and MORGAN database [47].

Our tool is reasonably compared with BOLSIG+. The results of *Mean Electron Energy* (eV) is shown in Table 6.3, and the plot of **EEDF** are shown in Figure 6.1 and Figure 6.2. A comparison of electron impact reaction rate coefficients between BOLSIG+ and our tool is shown in Figure 6.3. The calculation of the elastic loss energy coefficient of momentum transfer process of electron - CH_4 and electron - Ar are shown in Figure. 6.4a and Figure 6.4b, respectively. The total inelastic loss energy coefficient is shown in Figure. 6.4c. Finally, the deposited energy coefficient of electron is shown in Figure. 6.4d.

6.9 Summary

So, the BE solver that we have developed is able to calculate reasonably the Electron Energy Distribution Function (EEDF). Then, EEDF used to determine the information of plasma consisting of the electron impact reaction rate coefficient, the elastic loss energy coefficient, inelastic loss energy coefficient, and deposited energy coefficient. All these results are reliable when compared with BOLSIG+.

This tool will be useful for solving the implicit electron temperature equation later, by using a iteration method.

Table 6.1: The Parameters for BE solver

Parameters	**Value**
Gas Temperature (K)	$400K$
Gas Composition	CH_4: 0.5 - Ar: 0.5
Electric field / N (Td)	from 100 Td to 2000 Td
Angular Frequency / N ($m^3 \cdot rad/s$)	0.10000E-11

Table 6.2: Electron Impact Reactions

No.	**Electron Impact Reactions**	**Threshold Energy (eV)**	**Type of Reaction**
1	$E + Ar \longrightarrow E + Ar$	-	Momentum Transfer
2	$E + Ar \longrightarrow E + Ar \cdot$	11.5	Excitation
3	$E + Ar \longrightarrow Ar^+ + 2E$	15.8	Ionization
4	$E + CH_4 \longrightarrow CH_3 + H^-$	7.7	Dissociation Attachment
5	$E + CH_4 \longrightarrow CH_2 + {H_2}^-$	9.0	Dissociation Attachment
6	$E + CH_4 \longrightarrow E + CH_4$	-	Momentum Transfer
7	$E + CH_4 \longrightarrow E + CH_4(v_{24})$	0.162	Vibrational Excitation
8	$E + CH_4 \longrightarrow E + CH_4(v_{13})$	0.361	Vibrational Excitation
9	$E + CH_4 \longrightarrow E + CH_4 \cdot$	9.0	Excitation
10	$E + CH_4 \longrightarrow E + CH_4 \cdot$	10.0	Excitation
11	$E + CH_4 \longrightarrow E + CH_4 \cdot$	11.0	Excitation
12	$E + CH_4 \longrightarrow E + CH_4 \cdot$	12.0	Excitation
13	$E + CH_4 \longrightarrow {CH_4}^+ + 2E$	12.6	Ionization
14	$E + CH_4 \longrightarrow H + {CH_3}^+ + 2E$	14.3	Dissociation Ionization

Table 6.3: The comparison of Mean Electron Energy between Bolsig+ and our code

Electric field / N (Td)	**Mean Electron Energy (eV)**		**Error**
	BOLSIG+	Our Code	
100	0.0948	0.0945	0.32%
200	0.114	0.1146	0.53%
300	0.170	0.1457	14.29%
400	0.472	0.4926	4.36%
500	1.21	1.0041	17.02%
600	2.10	2.0705	1.40%
700	2.88	2.8720	0.28%
800	3.49	3.4931	0.09%
900	4.01	4.0079	0.05%
1000	4.46	4.4587	0.03%
1100	4.87	4.8711	0.02%
1200	5.26	5.2586	0.03%
1300	5.63	5.6300	0.00%
1400	5.99	5.9904	0.01%
1500	6.34	6.3435	0.06%
1600	6.69	6.6914	0.02%
1700	7.03	7.0357	0.08%
1800	7.37	7.3778	0.11%
1900	7.71	7.7186	0.11%
2000	8.05	8.0587	0.11%

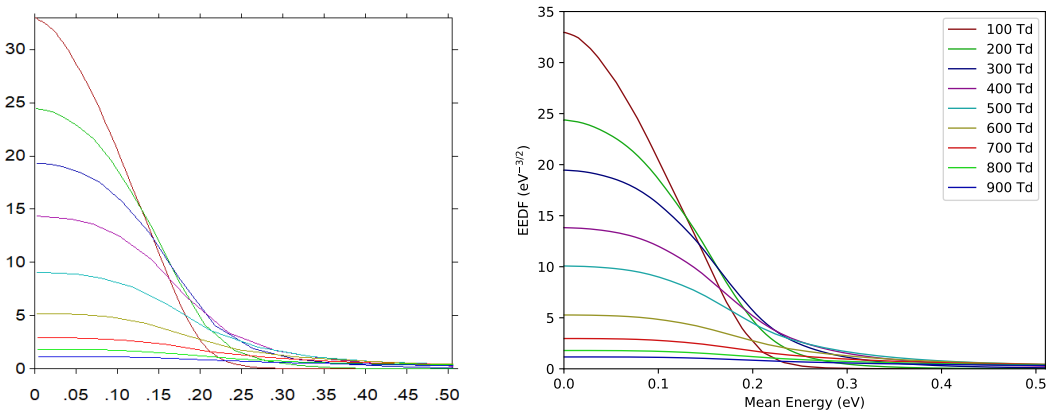

(a) (b)

Figure 6.1: Plot of EEDF correspond to E/N from 100Td to 900 Td. (a) Result of BOLSIG+ (b) Result of our code

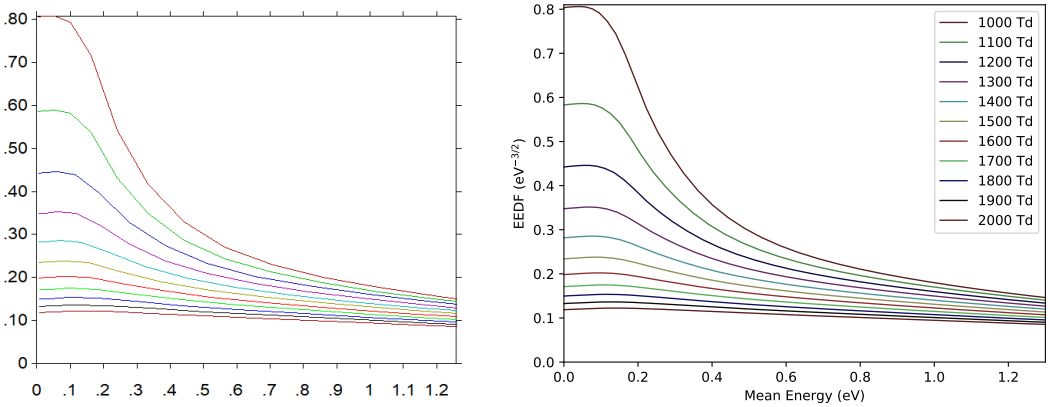

(a) (b)

Figure 6.2: Plot of EEDF correspond to E/N from 1000Td to 2000 Td. (a) Result of BOLSIG+ (b) Result of our code

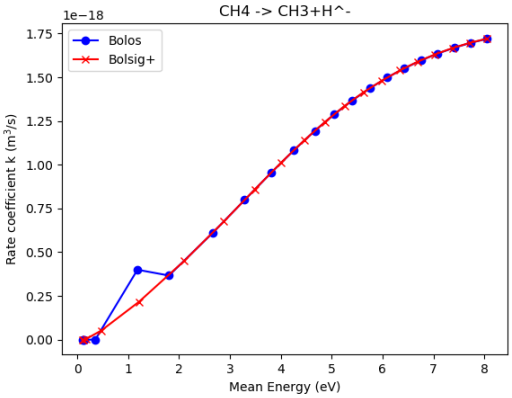

(a) Attachment:
$E + CH_4 \longrightarrow CH_3 + H^-$

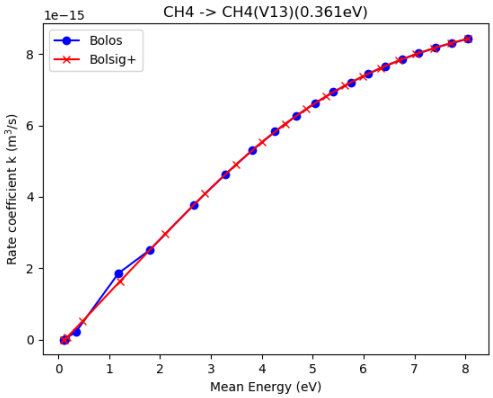

(b) Vibrational Excitation:
$E + CH_4 \longrightarrow E + CH_4(v_{13})$

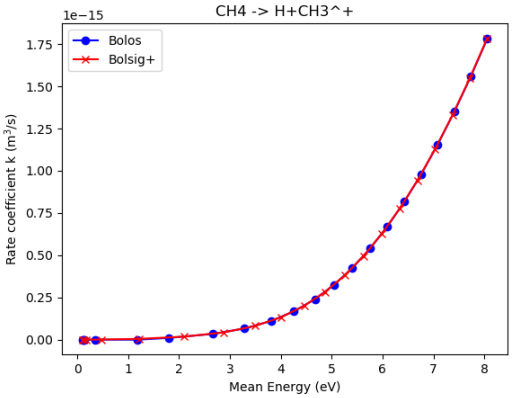

(c) Dissociation Ionization:
$E + CH_4 \longrightarrow H + CH_3^+ + 2\,E$

Figure 6.3: Comparison of rate coefficients between BOLSIG+ and Our tool

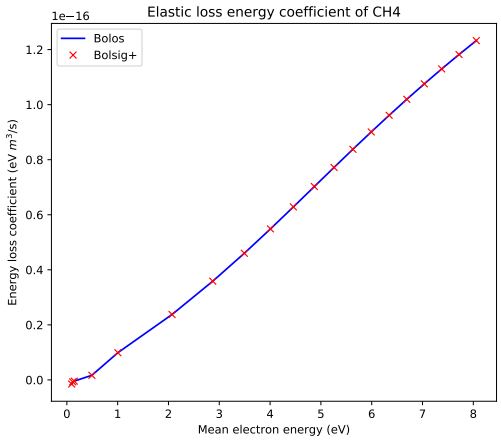

(a) Elastic loss energy coefficient of process: $E + CH_4 \longrightarrow E + CH_4$

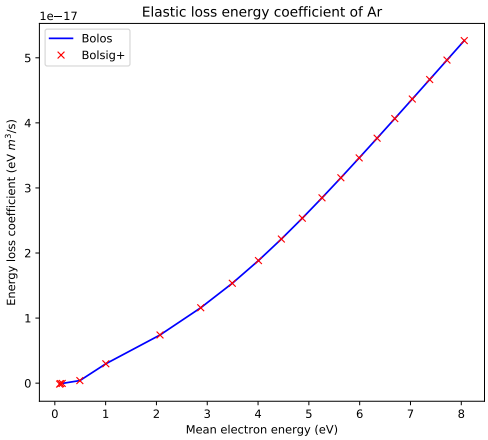

(b) Elastic loss energy coefficient of process: $E + Ar \longrightarrow E + Ar$

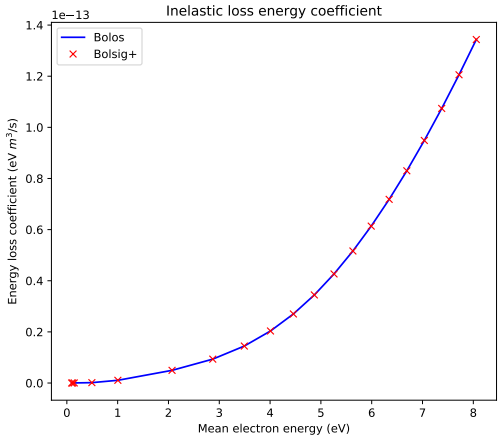

(c) Total inelastic loss energy coefficient

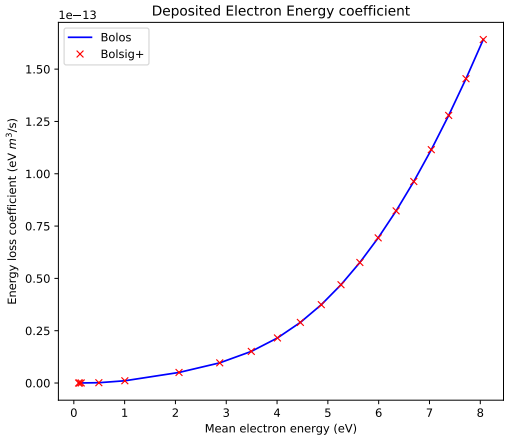

(d) Deposited energy coefficient of electron

Figure 6.4: Comparison of energy coefficient of plasma between BOLSIG+ and Our tool.

Chapter 7

Conclusion and Perspectives

We will summary the achievement and the limitations of our work as well as the next works to complete our numerical tool in this chapter.

In this study, we have validated our 0D model which could simulate a PRF reactor with presence of a catalyst bed in *Chapter 4*. The results are highly fit to numerical results of *Delgado et al* using a 1D model of commercial software DETCHEM. And in *Chapter 6*, we have developed a BE solver, which operates in Python environment, from an open source code - BOLOS based on the algorithm of *Hagelaar and Pitchford*. It provides the steady state of BE equation for electron in uniform or oscillating electric field, by using a two-term expansion and an exponential scheme commonly used for convection - diffusion problems. The **EEDF** got from BE solver is used to determined the rate coefficient of electron impact reactions, which is highly close with BOLSIG+. Furthermore, we also have determined the loss and deposited energy coefficient of plasma with the high reliability.

Up till now, we still have not had a GUI interface for our tool, all process are conducted by changing the code. Although, the change of parameters in code don't take a lot of time, that is still a limitation. Luckily, creating a GUI interface is not too difficult, it

is completely possible to solve when we build a complete numerical tool later.

In a nut shell, plasma is a complex phenomenon in practice, and simulation of plasma is really more complex. Thus, a 0D reactor model is the easiest way to take the chemical plasma into account, that was why a 0D model is used in our study. In the future, in order to coupling the affect of plasma into reactor model, we have to concentrate on studying the plasma model and the numerical method for proposing a suitable numerical strategy solving the two-temperature model. That is not easy, and I strongly believe that the challenges have just begun!

"Accept the challenges so that you can feel the exhilaration of victory"

— George S.Patton

Bibliography

[1] J. P. Rafferty, *Superstorm Sandy*, 2012 (accessed Jun 9, 2020). https://www.britannica.com/event/Superstorm-Sandy.

[2] S. Gibbens, *Hurricane Sandy, explained*, Feb 11, 2019 (accessed Jun 9, 2020). https://www.nationalgeographic.com/environment/natural-disasters/reference/hurricane-sandy/.

[3] M. Allen, O. Dube, W. Solecki, F. A. Durand, W. Cramer, S. Humphreys, M. Kainuma, J. Kala, N. Mahowald, Y. Mulugetta, R. Perez, M. Wairiu, , and K. Zickfeld., "In an ipcc special report on the impacts of global warming of 1.5°c above pre-industrial levels and related global greenhouse gas emission pathways," *Framing and Context*, pp. 49–91, 2018. [Online available].

[4] U. S. Government, *Greenhouse Gas Emissions*, 2018 (accessed Jun 9, 2020). https://www.epa.gov/ghgemissions/overview-greenhouse-gases.

[5] Eurostat, *Energy statistics: an overview*, 2020 (accessed Jun 10, 2020). https://ec.europa.eu/eurostat/statisticsexplained.

[6] J. R. Rostrup-Nielsen, "New aspects of syngas production and use," *Catalysis Today*, pp. 159–164, 2000. DOI: 10.1016/S0920-5861(00)00455-7.

[7] J. D. Medrano-García, R. Ruiz-Femenia, and J. A. Caballero, "Multi objective optimization of a carbon dioxide utilization superstructure for the synthesis of formic and acetic acid," *Computer Aided Chemical Engineering*, vol. 43, pp. 1419–1424, 2018. DOI: 10.1016/S0920-5861(00)00455-7.

[8] J. Xu and G. F. Froment, "Methane steam reforming, methanation and water-gas shift: 1. intrinsic kinetics," *AIChE Journal*, vol. 35, pp. 88–96, 1989.

[9] M. Bradford and M. A. Vannice, "Co2 reforming of ch4," *Catalysis Reviews*, pp. 1–42, 2007. DOI: 10.1081/CR-100101948.

[10] K. Wittich, M. Kramer, N. Bottke, and S. A. Schunk, *Review paper: Catalytic dry reforming of methane: Insights from model systems*. DOI: 10.1002/cctc.201902142.

[11] A. Duruphy, A. Casalot, A. Jaubert, and C. Mesnil, *Chimie 1re annee*. Hachette superieur, 1999.

[12] T. Poinsot and D. Veynante, *Theoretical and Numerical Combustion*. R.T. Edwards, Inc, 2005.

[13] T. Poinsot, *Cerfacs: Combustion Course*, (accessed Jun 10, 2020). `http://elearning.cerfacs.fr/combustion/index.php`.

[14] H. S. Fogler, *Elements of Chemical Reaction Engineering*. Pearson Education, Inc, 2016.

[15] M. E. Coltrin, R. J. Kee, and F. M. Rupley, "Surface chemkin:a general formalism and software for analyzing heterogeneous chemical kinetics at a gas-surfaceinterface," *Chemical Kinetics*, vol. 23, pp. 1111–1128, 1991.

[16] R. J. Kee, M. E. Coltrin, P. Glarborg, and H. Zhu, *CHEMICALLY REACTING FLOW: Theory, Modeling, and Simulation*. John Wiley & Sons, Inc, 2018.

[17] D. G. Goodwin, R. L. Speth, H. K. Moffat, and B. W. Weber, *Cantera: An Object-oriented Software Toolkit for Chemical Kinetics, Thermodynamics, and Transport Processes*. Accessed June 2020, `https://cantera.org`.

[18] E. Meeks and J. W. Shon, "Modeling of plasma-etch processes using well stirred reactor approximations and including complex gas-phase and surface reactions," *Transactions on Plasma Science*, vol. 23, 1995.

[19] A. H. Khoja, M. Tahir, and N. A. S. Amin, "Recent developments in non-thermal catalytic dbd plasma reactor for dry reforming of methane," *Energy Conversion and Management*, pp. 529–560, 2019.

[20] *ANSYS Chemkin Theory Manual 17.0 (15151), Reaction Design: San Diego*, 2015.

[21] R. J. Kee, F. M. Rupley, and E. Meek, *Chemkin-III: A Fortran Chemical Kinetics Package for the Analysis of Gasphase Chemical and Plasma Kinetics*. SAND 96-8216, 1996.

[22] *Surface reactions: Catalytic oxidation and steam/dry reforming of methane over nickel*. `https://www.detchem.com/mechanisms`.

[23] A. C. Hindmarsh, P. N. Brown, K. E. Grant, S. L. Lee, R. Serban, D. E. Shumaker, and C. S. Woodward, "SUNDIALS: Suite of nonlinear and differential/algebraic equation solvers," *ACM Transactions on Mathematical Software (TOMS)*, vol. 31, no. 3, pp. 363–396, 2005.

[24] E. Suli and D. F. Mayers, *An Introduction to Numerical Analysis*. Cambridge University Press, 2003.

[25] A. ISERLES, *A First Course in the Numerical Analysis of Differential Equations - Second Edition*. Cambridge University Press, 2009.

[26] K. H. Delgado, L. Maier, S. Tischer, A. Zellner, H. Stotz, and O. Deutschmann, "Surface reaction kinetics of steam and co2 reforming as well as oxidation of methane over nickel based catalysts," *Catalysts*, pp. 871–904, 2015. DOI: 10.3390/catal5020871.

[27] G. P. Smith, D. M. Golden, M. Frenklach, N. W. Moriarty, M. G. Boris Eiteneer, C. T. Bowman, R. K. Hanson, S. Song, J. William C. Gardiner, V. V. Lissianski, , and Z. Qin, *GRI-MECH 3.0*. Available at: `http://www.me.berkeley.edu/gri_mech/`.

[28] A. Burcat's, *Ideal Gas Thermodynamic Data in Polynomial form for Combustion and Air Pollution Use*, 2006. Accessed on June 2020, `http://garfield.chem.elte.hu/Burcat/burcat.html`.

[29] *Chemical-Kinetic Mechanisms for Combustion Applications*. San Diego Mechanism web page, Mechanical and Aerospace Engineering (Combustion Research), University of California at San Diego, `http://combustion.ucsd.edu`.

[30] *Chemistry Web Book*. `https://webbook.nist.gov/`.

[31] K. H. Delgado, H. Stotz, L. Maier, S. Tischer, A. Zellner, and O. Deutschmann, "Surface reaction kinetics of steam- and co2-reforming as well as oxidation of methane over nickel-based catalysts," *Catalysts*, vol. 5, pp. 871–904, 2015.

[32] P. M. Bellan, *Fundamentals of Plasma Physics*. CUP, 2004.

[33] A. Fridman, *Plasma Chemistry*. Cambridge University Press, 2008.

[34] N.N.Misra, "The contribution of non-thermal and advanced oxidation technologies towards dissipation of pesticide residues," *Trends in Food Science & Technology*, vol. 45, pp. 229–244, 2015. DOI: 10.1016/j.tifs.2015.06.005.

[35] U. Kogelschatz, "Dielectric-barrier discharges: Their history, discharge physics, and industrial applications," *Plasma Chemistry and Plasma Processing*, vol. 23, pp. 1–46, 03 2003.

[36] R. Tiňo, K. Vizárová, and F. Krčma, *Nanotechnologies and Nanomaterials for Diagnostic, Conservation and Restoration of Cultural Heritage*. Elsevier, 2019.

[37] J. C. Whitehead, *Cold Plasma in Food and Agriculture*. Elsevier Inc, 2016.

[38] N. BOUCHOUL, *THESE: Valorisation du dioxyde de carbone par couplage plasma non-thermique et catalyse*. 2019.

[39] J. Howard, *Introduction to Plasma Physics C17 Lecture Notes*. 2002. Australian National University.

[40] W. Morgan and B. Penetrante, "Elendif: A time-dependent boltzmann solver for partially ionized plasmas," *Computer Physics Communications*, vol. 58, pp. 127–152, 199. DOI: 10.1016/0010-4655(90)90141-M.

[41] G. J. M. Hagelaar and L. C. Pitchford, "Solving the boltzmann equation to obtain electron transport coefficients and rate coefficients for fluid models," *Plasma Sources Science and Technology*, vol. 14, pp. 722–733, 2005.

[42] D. Loffhagen, R. Winkler, and G. L. Braglia, "Two-term and multi-term approximation of the nonstationary electron velocity distribution in an electric field in a gas," *Plasma Chemistry and Plasma Processing*, vol. 16, 1996.

[43] *LXCAT: Plasma Data Exchange Project*. `www.lxcat.net`.

[44] D. L. Scharfetter and H. K. Gummel, "Large-signal analysis of a silicon read diode oscillator," *IEEE Transactions on Electron Devices*, vol. 16, no. 1, pp. 64–77, 1969.

[45] A. Luque, *Bolos: A library to solve the Boltzmann equation*, 2018. `https://pypi.org/project/bolos/`.

[46] *PHELPS database*. `http://www.lxcat.laplace.univ-tlse.fr`, retrieved April 20, 2020.

[47] *MORGAN database*. `http://www.lxcat.laplace.univ-tlse.fr`, retrieved April 20, 2020.

Appendix A: Code for Study Case Steam Reforming

Here is a example code for study case of Steam Reforming. For other study case, we just modify the composition of gas.

```
import numpy as np
import cantera as ct
import csv

# unit conversion factors to SI
cm = 0.01
minute = 60.0

# Set the initial value of flow
t0 = 298.15
pressure = 0.986923267* ct.one_atm  # 1bar pressure
Q = 4e3 * cm**3 / minute            # Flow rate 4 slpm

#########################################################
################## DIMENSION OF REACTOR #################
#########################################################
length = 2.7 * cm           # Catalyst bed length
dint = 1 *cm                # Inner diameter of reactor
area = np.pi * dint**2 /4   # Catalyst bed area
cat_area_per_vol = 9.85e6   # Catalyst particle surface area per unit volume
porosity = 0.42             # Catalyst bed porosity
# The PFR will be simulated by a chain of 200 stirred reactors.
NReactors = 201

#########################################################
# INPUT FILE CONTAINING THE SURFACE REACTION MECHANISM #
#########################################################
cti_file = 'Ni_surf_mech.cti'
composition = 'CH4:1.6, H2O:2, N2:96.4'

# import the gas model and set the initial conditions
gas = ct.Solution(cti_file, 'gas')
gas.TPX = t0, ct.one_atm, composition # This condition is used to get the total mass
    flow rate
# Set the mass flow rate before simulating.
mass_flow_rate = Q * gas.density

rlen = length/(NReactors-1)         # Length of one reactor
rvol = area * rlen * porosity       # Volume of one reactor
cat_area = cat_area_per_vol * rvol  # catalyst area in one reactor

#########################################################
################### DEFINE A SOLVER #####################
#########################################################
```

```
def solve(gas,t):
    # Set parameter of gas at operating condition
    gas.TPX = t, pressure, composition
    # Define a interface between Ni surface and Gas.
    surf = ct.Interface(cti_file,'Ni_surf', [gas])
    surf.TP = t, pressure

    # Set a steady state of surface
    TDY = gas.TDY
    cov = surf.coverages
    gas.TDY = TDY

    # create a new reactor & set volume for that reactor
    r = ct.IdealGasReactor(gas, energy='off')
    r.volume = rvol

    # create a reservoir to represent the reactor immediately upstream. Note that the
    gas object is set already to the state of the upstream reactor
    upstream = ct.Reservoir(gas, name='upstream')

    # create a reservoir for the reactor to exhaust into. The composition of this
    reservoir is irrelevant.
    downstream = ct.Reservoir(gas, name='downstream')

    # Add the reacting surface to the reactor. The area is set to the desired catalyst
    area in the reactor.
    rsurf = ct.ReactorSurface(surf, r, A=cat_area)

    # The mass flow rate into the reactor will be fixed by using a MassFlowController
    object.
    m = ct.MassFlowController(upstream, r, mdot=mass_flow_rate)

    # We need an outlet to the downstream reservoir. This will determine the pressure in
     the reactor. The value of K will only affect the transient pressure difference.
    v = ct.PressureController(r, downstream, master=m, K=1e-5)

    # create a reactor network for performing time integration
    sim = ct.ReactorNet([r])

    # set maximum test fail number, relative and absolute tolerances for the simulation
    sim.max_err_test_fails = 20
    sim.rtol = 1.0e-9
    sim.atol = 1.0e-21

    # define an information storing array
    states = ct.SolutionArray(gas)

    # iterate through the PFR cells
    for n in range(NReactors):
        # Set the state of the reservoir to match that of the previous reactor
        gas.TDY = r.thermo.TDY
        upstream.syncState()
        # integrate the reactor forward in time until steady state is reached
        sim.reinitialize()
        sim.advance_to_steady_state()
        # Append the state of gas
        states.append(gas.state)
    print('Temperature of Gas :', t)
    MolFrac_CH4 = states('CH4').X
    MolFrac_CO2 = states('CO2').X
    MolFrac_CO  = states('CO').X
    MolFrac_H2  = states('H2').X
    MolFrac_H2O = states('H2O').X
    rs = np.zeros(5)
    rs[0] = MolFrac_CH4[-1]*100
    rs[1] = MolFrac_CO2[-1]*100
    rs[2] = MolFrac_CO[-1]*100
```

```
    rs[3] = MolFrac_H2[-1]*100
    rs[4] = MolFrac_H2O[-1]*100
    return rs

n = 81
Tem = np.linspace(400,1200,n)   # Range of temperature considered
############################################################
############### SOLVE AND SAVE RESULT ####################
############################################################
with open('SR_T.csv', mode='w', newline='') as csv_file:
    fieldnames = ['T', 'CH4', 'CO2', 'CO', 'H2','H2O']
    writer = csv.DictWriter(csv_file, fieldnames=fieldnames)
    writer.writeheader()
    for i in range(n):
        rs = solve(gas,Tem[i])
        writer.writerow({'T': Tem[i], 'CH4': rs[0], 'CO2': rs[1], 'CO': rs[2], 'H2': rs
    [3], 'H2O': rs[4]})
```

Appendix B: Code of BE Solver

```
import numpy as np
import scipy.constants as co
import matplotlib.pyplot as plt
from bolos import parser, grid, solver2
import csv
np.seterr(divide='ignore', invalid='ignore')
""" This program use own 'solver2.py' library was developed based on the algorithm of G. J. M. Hagelaar and L. C. Pitchford.
    'solver2.py' file need to copy to the Bolos package in order to use our tool"""
# Create an energy grid for Boltzmann Solver
# This energy grid has unit in eV
gr = grid.QuadraticGrid(0, 20, 200)
bsolver = solver2.BoltzmannSolver(gr)

# Import data file, which contains the cross section data.
with open('CrossSection.dat') as fp:
    processes = parser.parse(fp)
processes = bsolver.load_collisions(processes)
bsolver.target['CH4'].density = 0.5
bsolver.target['Ar'].density = 0.5

##################################################
############### INPUT PARAMETER ##################
##################################################
# We have electric field:
# E = E0 * exp (i * Omega * t)
bsolver.OmegaN = 0.10000E-11        # Omega / N
bsolver.kT = 400 * co.k / co.eV     # Gas - Temperature 400 K

# GUESS initial value by Maxwell distribution function.
# Here we are starting with an electron temperature of 6 eV
f0 = bsolver.maxwell(6.0)
mean_max = bsolver.mean_energy(f0)

##################################################
############### DEFINE A SOLVER ##################
##################################################
def EEDF_AC(EN, f0):
    """ This function used to calculate the EEDF for oscillating electric field"""
    bsolver.grid = gr
    bsolver.EN = EN * solver2.TOWNSEND
    # After change any parameter we must initial the solver
    bsolver.init()
    f1 = bsolver.converge(f0, maxn=200, rtol=1e-4)
    mean1 = bsolver.mean_energy(f1)
    print('E/N = %.0f' % EN)
    # print('Mean Energy 1 = %.4f  ' % (mean1))

    # Get new grid
    newgrid = grid.QuadraticGrid(0, 10 * mean1, 200)
    bsolver.grid = newgrid
    bsolver.init()
```

```
52
53      # Interpolate the previous EEDF over new grid
54      f2 = bsolver.grid.interpolate(f1, gr)
55      mean2 = bsolver.mean_energy(f2)
56
57      # Find final EEDF
58      f3 = bsolver.converge(f2, maxn=200, rtol=1e-5)
59      mean3 = bsolver.mean_energy(f3)
60      print('Mean Energy Final-EEDF = %.4f '  % mean3)
61
62      grid_EEDF = bsolver.cenergy
63      return f3, grid_EEDF, mean3
64  ##################################################
65  ############# DEFINE ENERGY TERM #################
66  ##################################################
67  def Power(EEDF,EN):
68      """ This function used to calculate the Deposited energy of electron coefficient"""
69      per_mobility = bsolver.perpendicular_mobility(EEDF)
70      power_electron = per_mobility * (EN * solver2.TOWNSEND)**2
71      return power_electron
72
73  def Q_loss_inelas(EEDF):
74      """ This function used to calculate the inelastic loss energy coefficient"""
75      Q_loss_inelas = 0
76      for t, k in bsolver.iter_inelastic():
77          target = k.target_name
78          product = k.product
79          threshold = k.threshold
80          k = bsolver.search(target, product)
81          rate = bsolver.rate(EEDF, k)
82          Q_loss_inelas = Q_loss_inelas + rate * k.target.density * threshold
83      return Q_loss_inelas
84
85  # Range of Electric field / Number of electron - E0/N
86  # E = E0 * exp (i * Omega * t)
87  EN = np.linspace(100,2000,20)
88
89  mean = np.zeros_like(EN)
90  Q_source = []
91  Q_elas = []
92  Q_inelas = []
93  GAMMA = np.sqrt(2 * co.elementary_charge / co.electron_mass)
94  # Create two variables storing the elastic energy of CH4 and Ar
95  CH4 = []
96  Ar = []
97  plt.figure()
98  with open('rate_coefficient.csv', mode='w', newline='') as csv_file:
99      writer = csv.writer(csv_file)
100     # Write header of output file
101     a = ['Mean Energy (eV)']
102     for t, k in bsolver.iter_all():
103         text = str(k)
104         a.append(text[1:-1])
105     writer.writerow(a)
106     for i, ien in enumerate(EN):
107         EEDF, gr_EEDF, mean[i] = EEDF_AC(ien, f0)
108         plt.plot(gr_EEDF, EEDF, linewidth = 1, label='%.f Td' % i)
109         # Write data of Mean energy and rate constant for each reaction.
110         output = [mean[i]]
111         for t, k in bsolver.iter_all():
112             output.append(bsolver.rate(EEDF, k))
113         writer.writerow(output)
114
115         # Calculate the energy term of plasma
116         Q_source.append(Power(EEDF,ien))
117         Q_inelas.append(Q_loss_inelas(EEDF))
118
```

```
        # Calculate the elastic loss energy
        for t, k in bsolver.iter_elastic():
            target = k.target_name
            product = k.product
            k1 = bsolver.search1(target, product)
            print(k1)
            Q = bsolver.Elas_loss_power_coef(EEDF, k1, bsolver.kT)
            print('Loss Energy  = ',Q, '\n')
            if t.name == 'CH4':
                CH4.append(Q)
            else:
                Ar.append(Q)
        print('Absorbed Power of electron   = ', Q_source[i])
        print('Inelastic loss Power         = ', Q_inelas[i] , '\n')

with open('energy_coefficient.csv', mode='w', newline='') as csv_file:
    fieldnames = ['EN', 'Mean_Energy', 'Elastic_Loss_Energy_CH4', '
    Elastic_Loss_Energy_Ar', 'Inelastic_Loss_Energy', 'Electron_Deposited_Power']
    writer = csv.DictWriter(csv_file, fieldnames=fieldnames)
    writer.writeheader()
    for i in range(len(EN)):
        writer.writerow({'EN': EN[i], 'Elastic_Loss_Energy_CH4': CH4[i], '
    Elastic_Loss_Energy_Ar': Ar[i], 'Mean_Energy':mean[i], 'Inelastic_Loss_Energy':
    Q_inelas[i], 'Electron_Deposited_Power':Q_source[i]})
```